QATAR UNIVERSITY

COLLEGE OF ENGINEERING

FLEXURAL STRENGTHENING OF REINFORCED CONCRETE BEAMS USING FABRIC REINFORCED CEMENTITIOUS MATRIX SYSTEMS

BY

HOSSAMELDIN ABDOU M A EL SHERIF

A Thesis Submitted to

the Faculty of the College of Engineering

in Partial Fulfillment of the Requirements for the Degree of

Masters of Science in Civil Engineering

June 2019

COMMITTEE PAGE

The members of the Committee approve the Thesis of
HossamEldin ElSherif defended on 18/04/2019.

Prof. Usama Ebead
Thesis/Dissertation Supervisor

Dr. Khalid Naji
Committee Member

Prof. Khaldoon Bani-Hani
Committee Member

Dr. Neaz Sheikh
Committee Member

Approved:

Abdel Magid Hamouda , Dean, College of Engineering

ABSTRACT

ELSHERIF, HOSSAMELDIN, A., Masters : June : 2019,

Masters of Science in Civil Engineering

Title: Flexural Strengthening of Reinforced Concrete Beams Using Fabric Reinforced Cementitious Matrix Systems

Supervisor of Thesis: Prof. Usama, A, Ebead.

This thesis is an experimental study performed to investigate the effectiveness of near surface embedded (NSE) and the hybrid near surface embedded externally bonded (NSE/EB) fabric reinforced cementitious matrix (FRCM) systems for flexural strengthening of reinforced concrete (RC) beams in flexure. A total of twenty beams were prepared with the consideration of three test parameters: (a) FRCM material (polyparaphenylene benzobisoxazole (PBO)/carbon/glass); (b) strengthening technique (externally bonded (EB), NSE and NSE/EB); and (c) the longitudinal reinforcement ratio (0.5% representing flexure-deficient beams and 1.28% representing typical under-reinforced beams). The results show that NSE strengthening provides improved bond behavior between FRCM composite and concrete substrate. The strengthening led to gains in ultimate flexural loads ranging between 30.1% and 108.6%. It was concluded that both NSE and NSE/EB are a valid strengthening alternative to the traditional EB strengthening.

ACKNOWLEDGEMENT

First, I would like to thank Allah for his blessings and mercy. I would also like to thank my thesis advisor Professor Usama Ebead. The door to Prof. Ebead's office was always open whenever I ran into a trouble spot or had a question about my research or writing. He consistently allowed this work to be my own work but steered me in the right direction whenever he thought I needed it. My thanks also extend to Eng. Siju Joseph for his help in testing the specimens.

TABLE OF CONTENTS

ACKNOWLEDGEMENT iv

LIST OF TABLES viii

LIST OF FIGURES ix

Chapter 1: Introduction 1

1.1 Research problem and objectives 1

1.2 Background 1

1.2.1 Jacketing and Ferrocement 2

1.2.2 Fiber Reinforced Polymers (FRP) 2

1.2.3 Fabric Reinforced Cementitious Matrix (FRCM) 3

1.3 Thesis outline 4

Chapter 2: Literature Review 5

2.1 Current research campaign on FRCM 5

2.1.1 FRP Shear Strengthening 5

2.1.2 FRCM Bond Behaviour 6

2.1.3 FRCM Flexural Strengthening 6

2.1.4 FRCM Shear Strengthening 7

2.1.5 Corrosion Damaged Beams 8

2.2 Previous studies on the flexural strengthening of RC beams using FRCM 9

2.3 Substrate surface preparation 12

2.4 Effect of using multiple FRCM fabric layers 13

Chapter 3: Experimental Details 15
3.1 Concrete and Steel Properties 15
3.2 FRCM Properties 16
3.3 Test Matrix 17
3.4 Preparation of Specimens 21
3.4.1 NSE-FRCM Strengthened Beams 22
3.4.2 EB-FRCM Strengthened Beams 25
3.4.3 Hybrid NSE/EB-FRCM Strengthened Beams 26
3.5 Test setup and instrumentation 29
Chapter 4: Results and Discussion 32
4.1 Results 32
4.1.1 Equivalent Stiffness Factor 32
4.1.2 Load-Deflection Relationships 35
4.2 Discussion 39
4.2.1 Load Carrying Capacity 39
4.2.2 Deformational Characteristics 41
4.2.3 Failure Modes and Cracking Patterns 43
Chapter 5: Theoretical Calculations 51
Chapter 6: Conclusions 55
References 57
Appendixes 62

Appendix A: Theoretical load carrying capacity example calculation.....62

LIST OF TABLES

Table 1 Steel reinforcement properties 15

Table 2 Mechanical and geometric properties of FRCM fabrics 17

Table 3 FRCM coupon tests results 17

Table 4 Test matrix 20

Table 5 Strain gages details 31

Table 6 Summary of test results 34

Table 7 Calculated load carrying capacity values 54

LIST OF FIGURES

Figure 1 Different surface preparation techniques 12

Figure 2 FRCM fabrics 16

Figure 3 Reinforcement details 18

Figure 4 Strengthening details 19

Figure 5 Strain gages installed on main steel reinforcement 21

Figure 6 steel cages placed in formwork 21

Figure 7 Concrete casting and finishing 22

Figure 8 NSE beams preparation 24

Figure 9 NSE-FRCM application 25

Figure 10 Hybrid specimens roughened surface 26

Figure 11 Hybrid NSE/EB specimens strengthening 28

Figure 12 Test setup and instrumentation 29

Figure 13 Specimen C-N-H during testing 30

Figure 14 TML data logger 31

Figure 15 Initial and post-cracking stiffness values evaluation 35

Figure 16 Load-deflection relationships for Group 1 specimens 36

Figure 17 Load-deflection relationships for Group 2 specimens 37

Figure 18 Load-deflection relationships for Group 3 specimens 38

Figure 19 Gain in P_u vs β^f 40

Figure 20 Reference specimens cracking patterns 44

Figure 21 Group 1 Specimens cracking patterns 45

Figure 22 Group 2 Specimens cracking patterns 46

Figure 23 Group 3 Specimens cracking patterns 47

Figure 24 Failure modes 50

CHAPTER 1: INTRODUCTION

1.1 Research problem and objectives

Focus has increased recently on strengthening reinforced concrete structures that deteriorate due to aging, corrosion of steel reinforcing bars, excessive loading, or severe environmental conditions. The strengthening of RC structures has been successfully implemented using fabric reinforced cementitious matrix (FRCM) systems for the flexure strengthening of RC beams. There is, however, a problem of premature debonding which is observed in high fabric strength FRCM systems which does not allow full utilization of the strengthening material. It has also been a problem in FRCM systems to use multiple layers for strengthening, where using more than two layers causes premature failure in the strengthened beams. This work aims to counter the problem of premature failure by investigating the relatively new concept of near surface embedded (NSE) strengthening where the strengthening material is embedded within the concrete cover at the soffit of the beam thus allowing the FRCM to be better utilized. Three different types of FRCM systems have been investigated, namely: Carbon, Polyparaphenylene Benzobisoxazole (PBO), and Glass. The potential of combining both NSE strengthening and the traditional externally bonded (EB) methods resulting in the hybrid near surface embedded/externally bonded (NSE/EB) is also examined in this work to investigate the efficient application of multiple FRCM layers in flexure. Part of the results of this work have been successfully published proving that it is a viable strengthening application [1].

1.2 Background

Reinforced concrete (RC) is the most commonly used construction material in many parts of the world due to its versatility and advantageous properties. However, the lifespan of RC structures can be significantly reduced due to a number of factors such as harsh weather conditions, excessive loads and chloride attacks. These factors

cause the development of cracks on the concrete surface thus accelerating the corrosion of the reinforcing steel bars. This necessitates strengthening to recover the structures original strength or prolong its lifespan. Other factors such as environmental disasters may cause RC structures to be deficient and not fit for use. Therefore, the decision must be made to either repair the structure or demolish it. Strengthening an RC structure can also be done to accommodate different uses or to make the structure compliant with new design codes. Multiple strengthening systems have been developed for RC structures, some of which are summarized and presented below.

1.2.1 Jacketing and Ferrocement

One of the earliest strengthening systems used is jacketing. This involves enlarging the concrete section with concrete and steel reinforcement. Jacketing can be used to enhance the capacity of beams, slabs, and columns to increase their strength and is most commonly used in strengthening RC columns. The use of jacketing for strengthening entails the reduction of the available space due to section enlargement, long installation time associated with the manual work involved and concrete curing, and the added weight of the enlarged sections.

Another common strengthening method is the use of ferrocement. Ferrocement consists of steel wire meshes applied externally on RC elements using cement mortars. The advantages of ferrocement are the low self-weight, ease of application, and no need for formwork. Ferrocement has also been proven to be a viable strengthening option where live loads cannot be fully removed during the strengthening process [2].

1.2.2 Fiber Reinforced Polymers (FRP)

As an alternative to traditional strengthening techniques such as jacketing and ferrocement, fiber reinforced polymer (FRP) systems have been introduced in the past decades. Having such advantageous properties as corrosion resistance, high strength-

to-weight ratio, and ease of application [3]. FRP can be applied as \externally bonded (EB) using epoxy, or mechanically fastened (MF) using anchors for the strengthening of RC elements. It proved to be successful for the strengthening of RC beams in both flexure [4] and shear [5] and. FRP can also be applied as near surface mounted (NSM) using FRP rods embedded within the concrete cover of the RC beams to enhance their flexural or shear capacities [6]. The FRP sheets or strips are usually applied using organic epoxy resins as the bonding agent which has the disadvantages of poor behavior at high temperatures, low glass transition temperatures, inability to be applied on humid surfaces, lack of vapor permeability, and incompatibility with the concrete substrates [7].

1.2.3 Fabric Reinforced Cementitious Matrix (FRCM)

To counter the deficiencies of FRP strengthening systems, fabric reinforced cementitious mortar (FRCM) systems have been recently developed. FRCM systems consist of open mesh textiles sandwiched between layers of inorganic cementitious matrix and are externally bonded to the RC elements. FRCM is also known as textile reinforced concrete (TRC) and textile reinforced mortar (TRM). The use of the inorganic matrix circumvents the disadvantages associated with the use of organic resins in FRP systems. FRCM systems offer multiple advantages such as compatibility with the concrete substrate, vapor permeability, ease of application using traditional plastering tools, ability to be applied on wet surfaces, ductile behavior, improved fire resistance [8]. FRCM strengthening has been proven successful for the strengthening of RC beams in both shear [9] and flexure [10].

1.3 Thesis outline

- Chapter 2: Literature Review: In this chapter, the relevant literature to flexure strengthening of RC beams is presented.
- Chapter 3: Experimental Details: The test matrix, test specimens preparation, material properties, testing setup and procedure, and data collection details are all explained in this chapter.
- Chapter 4: Results and Discussion: The resulting data and observations including load-deflection relationships, ultimate capacities, deflections, failure patterns, and failure modes are presented and investigated with reference to the different testing parameters.
- Chapter 5: Theoretical Calculations: The capacities of the specimens are calculated using the ACI code equations and compared with the experimental results.
- Chapter 6: Conclusion: This chapter summarizes the outcomes of the work and presents the main findings and conclusions drawn from this work.

CHAPTER 2: LITERATURE REVIEW

2.1 Current research campaign on FRCM

This work is part of a campaign on RC beam strengthening in both shear [11–13]and flexure [14]. In this campaign, new concepts are developed concerning shear and flexural strengthening where the interaction between strengthening material and reinforcement is examined. Multiple FRCM systems are also examined along with different strengthening schemes. Bond behavior and strength are investigated through pull-off and bond tests [15]. The FRCM composites were also characterized by performing tensile characterization tests on different FRCM systems. Another point of focus is the strengthening of corroded beams where specimens were subjected to accelerated corrosion and then strengthened to examine the FRCM strengthening [16–18]. The studies also examined alternative strengthening techniques such that strengthening is more viable in developing countries. These studies and findings are summarized in this section.

2.1.1 FRP Shear Strengthening

Ebead and Saeed [11] examines the interaction between the external FRP strengthening and internal shear reinforcement. The study analyzes both experimental and numerical results developed from finite element modeling. The tested specimens were strengthened using mechanically fastened (MF), externally bonded (EB), and hybrid mechanically fastened/externally bonded (MF/EB) techniques. It was observed that the average increase in load carrying capacity for beams without stirrups in the critical shear span was 82.2%. This value dropped to 69.2% for strengthened beams where stirrups are provided within the critical shear span. The study concludes that as the effectiveness of the strengthening system increases and the ultimate load capacity due to the strengthening increases, the steel stirrups lose their effectiveness along the critical shear span. It was also shown that the use of the hybrid MF/EB system leads to

lower shear slip along the concrete/FRP interface which is related to the continuous anchorage provided by the fasteners.

2.1.2 FRCM Bond Behaviour

Younis and Ebead [15] investigated the bond behavior of three different FRCM systems (Polyparaphenylene benzobisoxazole (PBO), Carbon, and Glass) experimentally by preparing eighteen specimens with variable bond lengths and fabric plies. The prepared specimens were subjected to double-shear tests until failure. The results show that Carbon-FRCM provided more ductile failure at the concrete/FRCM interface compared to its Glass- and PBO-FRCM counterparts. The highest bond capacity was exhibited by PBO-FRCM strengthened specimens despite the observed brittle failure mode. It was also noted that a linear tendency was observed in the relationship between bond capacity and bond length where an increase in bond length resulted in an increase in bond capacity. The number of fabric plies was shown to be strongly related to the failure mode where the increase in the fabric plies caused an improvement in the concrete/FRCM interface such that the failure occurs at the fabric/matrix interface instead. The study also proposed an analytical model for predicting the bond capacity and the failure mode for the tested specimens which showed reasonable agreement with the experimental results.

2.1.3 FRCM Flexural Strengthening

The study performed by Ebead et. al. [14], reported on the effectiveness of FRCM for the enhancement of the flexural capacity and deformational characteristics of RC beams. twelve 2.5 meter long beams were fabricated and tested under four-point loading until failure. The test parameters were the FRCM system (PBO and carbon), the reinforcement ratio (0.72% and 1.27%), and the layers of FRCM fabric (1,2 and 3 layers) The work also included a second part that tested the FRCM composites by

tensile coupons to determine the tensile characteristics. The results show that the strengthened beams had increased flexural capacity by up to 77% for carbon FRCM and 27% for PBO FRCM. The material characterization also shows that the PBO FRCM had an axial stiffness that was equivalent to 50% of that of the C-FRCM for the same number of layers of fabric. It was also observed that PBO-FRCM strengthened beams showed more ductile behavior when compared to the C-FRCM counterpart. The failure modes ranged from fabric slippage, FRCM delamination and a combination of both.

2.1.4 FRCM Shear Strengthening

Externally bonded (EB) FRCM has since been used for both shear and flexure as a strengthening system. The traditional EB-FRCM system, however, is characterized by poor interfacial performance between FRCM and concrete which usually leads to premature debonding, especially for thicker FRCM composites. This was observed in the performed studies in this campaign.

Younis et. al. [12] reported on the effectiveness of FRCM for shear strengthening of RC beams by analyzing experimental results obtained from testing sixteen beams under three-point loading strengthened with different configurations. The strengthening led to an average gain in load carrying capacity of 51% compared to the reference specimen. It was also observed that strengthened specimens exhibited more ductile behavior where the deflections at failure reached up to 2.4 times that of the reference specimen. While debonding type of failure was common among the strengthened beams, the strengthening configuration led to a change in the number and location of the debonding spots. The strengthened specimens also showed improvement in the crack widths where smaller widths were measured for the strengthened specimens. The smallest crack widths were measured in Carbon-FRCM strengthened

beams. The effect of anchorage on the FRCM system was also observed, however, it was noted to have a negligible effect on strength enhancement.

Wakjira and Ebead [13] proposed a new technique for shear strengthening صاثقث the FRCM composite is fully or partially embedded within the concrete cover with an external part labeled near surface embedded (NSE) and hybrid near surface embedded externally bonded (NSE/EB). The study experimentally examined thirteen beams strengthened with different FRCM systems (PBO, Carbon, and Glass), strengthening configurations, and number of fabric plies. It was observed that the proposed NSE/EB strengthening system led to substantial improvement in the shear capacity of the strengthened beams where the ultimate load carrying capacity reached up to 114% compared to the reference specimen. The average enhancement in the load capacities was observed to be 83.0%, 61.8%, and 71.6% for Carbon-, PBO, and Glass-FRCM strengthened specimens, respectively. It was also observed that no debonding was observed for specimens strengthened using only NSE strengthening. The NSE and NSE/EB strengthening techniques are investigated for flexure in this thesis.

2.1.5 Corrosion Damaged Beams

Studies performed also investigated the strengthening effect on RC beams subjected to corrosion. Elgazy et. al. [16] subjected RC beams to accelerated corrosion prior to strengthening them in flexure using FRCM composites to test the strengthening effect on corroded beams. The test parameters of the study were the number of fabric plies, the fabric type, and the strengthening scheme. The average steel mass loss due to corrosion was 22.7%. This did not have a significant effect on the flexural response of the beams where the maximum deficit in the yield and ultimate strengths of the corroded beams was 15% and 9%, respectively. The failure behaviour of the strengthened beams was governed by the type, amount, and anchoring scheme of

the FRCM strengthening composite rather than the corrosion damage. The strength gain ranged between 7-44% and 39-55% for PBO-FRCM, and Carbon-FRCM strengthened beams respectively, compared to that of the reference specimen.

Elghazy et. al. also studied on the effect of strengthening on corroded beams where the beams were subjected to accelerated corrosion resulting in average steel mass loss of 13% [17]. The corrosion damaged beams showed a restored load carrying capacity of between 105-144% and 130-152% when strengthened using PBO and carbon, respectively. The restored capacity was highly dependent on the FRCM system used, number of fabric plies, and the strengthening scheme utilized. It was also noted that beams repaired using PBO-FRCM displayed more ductile behavior than those repaired with Carbon-FRCM. RC beams were also subjected to intensive corrosion conditions both before and after strengthening is applied resulting in an average steel mass loss of 22.5% [18]. The results of the study show that strengthened specimens when exposed to corrosion, suffer 23% reduction in steel mass loss. The use of U-wrapping for FRCM strengthening was shown to be more efficient in reducing the corrosion rate. The strengthened specimens, when subjected to corrosive condition, mostly failed to meet crack width serviceability provisions of ACI-318-14.

2.2 Previous studies on the flexural strengthening of RC beams using FRCM

A detailed analysis of the previous research studies related to the flexural strengthening of RC beams using FRCM is conducted and presented in this section. Studies reporting on FRCM systems effectiveness are presented along with their limitations. The different surface preparation techniques and the effect of multiple FRCM fabric layer application are also analyzed.

The work done by El Sanadedy et. al. [19] reports on the effectiveness of FRCM flexural strengthening both experimentally and numerically. The test parameters in the

study were the type of mortar (polymer modified and non-polymer modified cementitious mortar) and the number of TRM layers (5 and 10 layers). Two control beams, three Basalt-TRM strengthened beams, and one CFRP strengthened beam were tested under four-point loading until failure. The TRM strengthening was done in a U-shaped technique. Among the conclusions of this study, it was observed that polymer modified cementitious matrix provides an improved bond between the concrete surface and TRM layers compared to normal cementitious mortars. The increase in flexural capacity in the strengthened beams ranged from 39% to 91% using basalt-TRM. It was also noted that TRM strengthening was more effective in terms of deflection and ductility while being less effective than the CFRP counterpart in enhancing the flexural strength. The polymer modified specimens failed due to fabric rupture while the non-polymer modified specimens failed due to plate end debonding.

Escrig et. al. [20] experimentally compared five different FRCM strengthening grids (basalt, carbon, glass, PBO, and steel) embedded in four different mortar matrices used for strengthening of RC beams against bending. The beams were strengthened using only one layer of FRCM fabric and tested under four-point loading until failure. It was concluded that FRCM strengthening let to an average increase of 135% in the flexural stiffness of the strengthened specimens which led to a decrease in ductility. FRCM strengthening also led to a delay in the appearance of the first crack during loading and reduces cracking. The strengthened specimens had the ultimate load carrying capacity increases by up to 23 % more than that of the control specimen. It was noted however that a specimen strengthened with a certain combination of grid and mortar did not reach the ultimate capacity of the control specimen which led to a conclusion that the ultimate capacity of strengthened beams is highly dependent upon the bonding capacity between grid and matrix.

The effect of FRCM strengthening on corroded T-beams was also investigated by El-Maaddawy and El Refai [21]. Eight T-beams were prepared and tested under four-point loading until failure. Seven specimens were subjected to corrosion and then strengthened using two different FRCM systems (basalt and carbon) and two different repair schemes (Internal and external). It was noted that the basalt FRCM did not recover the original un-corroded beam capacity even when four layers were applied. The full corroded beam capacity and ductility were however restored using two layers of carbon FRCM. The strength gain in the repaired corroded beams compared to the un-corroded control beam was up to 39%.

Experimental tests on FRCM strengthened slabs were performed by Schladitz et. al. [22] on slabs strengthened using Carbon-FRCM. Five RC slabs with dimensions 7 m × 1 m × 0.23 m were strengthened with up to four FRCM layers and tested under four-point loading until failure. It was observed that four layers of FRCM strengthening provided 3.5 times the reference unstrengthened load carrying capacity with decreased deflections at equal load levels. Loreto et. al., [23], also reported on the effectiveness of FRCM strengthening of RC slabs. The test parameters of the study were the concrete strength and the fabric plies (one and four plies). Eighteen slab specimens with dimensions 1.83 m × 0.305 m × 0.152 m were tested under three-point loading until failure. The resulting load carrying capacity enhancements were found to be 141 and 205% for low strength concrete specimens and 135 and 212% for high strength concrete specimens for one and four plie of FRCM, respectively.

2.3 Substrate surface preparation

ACI 549 guideline [24] recommends different concrete substrate surface preparation methods for FRCM strengthening which are as follows:

1) Abrading the concrete surface using sandblasting, hydrojetting, grinding, or similar methods. This allows the removal of fine grain concrete which may compromise the bond between the concrete substrate and FRCM composite. This is the most common technique among studies on FRCM strengthening [14,25–27] An example of a sandblasted surface is shown in Figure 1a.
2) Grinding form lines in the concrete surface and, in case of masonry joints, the excess mortar. An example of this is shown in Figure 1b. It was reported that both form lines and sandblasting were equally effective in ensuring an adequate bond between the substrate and FRCM [28]. However, this method is not very common among the performed studies.

(a)

(b)

Figure 1 Different surface preparation techniques[28]: a) Sandblasted surface, and b) form lines

While sandblasting or hydrojetting is the most commonly used substrate roughening method, it also constitutes safety hazards for the workers such as hearing and respiratory problems [29]. These hazards necessitate proper safety precautions prior to substrate preparation such as hearing protection and face masks.

An alternative substrate preparation method was proposed by Wakjira and Ebead that included the partial removal of the concrete cover and applying the FRCM composite within the created grooves [13]. This technique circumvents the safety hazards associated with sandblasting and provides an easier way of preparing the roughened surface. It also preserves the dimensions of the beam which may serve any architectural restrictions and replaces the concrete at the soffit of the beam which may be damaged in real applications. It is also reported that this method allows for improved bonding between the concrete substrate and FRCM composite in case of shear strengthening [13]. This can be further supported by Younis's work where it was reported that debonding was observed between the FRCM layer and concrete in beams strengthened with externally bonded FRCM (EB-FRCM) [12]. This technique, however, has not yet been investigated for flexural strengthening.

2.4 Effect of using multiple FRCM fabric layers

Another point of study in literature was the effect of multiple layers of fabrics in FRCM on the mode of failure of RC beams. The FRCM manufacturers recommend a certain mortar thickness per fabric ply, hence, the use of multiple plies increases the total FRCM thickness resulting in a premature failure in the FRCM/concrete bond [10,13,25]. Babaeidarabad et al. noted different failure modes prone to the number of layers of fabric. It was reported that beams strengthened using 1 ply and 4 plies of FRCM fabric experienced delamination on the fabric-matrix and FRCM-substrate levels, respectively [10]. Ombres also reported that the failure mode depended on the

volume fraction of fabric, where premature intermediate crack debonding occurred in beams with two or three plies of PBO fabric [25]. The work performed by Wakjira and Ebead proposed the hybrid near surface embedded externally bonded technique (NSE/EB) which allowed the application of multiple plies of fabric without the risk of premature failure by embedding the FRCM layers in the concrete cover [13].

These studies show the effectiveness of FRCM in the strengthening of RC beams in both shear and flexure. It also showed the ability to restore corroded RC elements to their load carrying capacity. The studies also show that the bond between FRCM composites and the concrete substrate is the governing factor for strengthening efficiency. The problem increases when applying multiple FRCM fabric layers which could cause premature debonding failure which does not allow full utilization of the FRCM composite.

CHAPTER 3: EXPERIMENTAL DETAILS

3.1 Concrete and Steel Properties

All beams were cast using the same batch of ready mix concrete to ensure similar characteristics. The proportions per cubic meter of concrete were 780 kg of sand, 950 kg of gravel, and 350 kg of ordinary Portland cement with a water/cement ratio of 0.45. Compression tests were carried out on 150 × 300 mm concrete cylinders in accordance with ASTM C39 [30] resulting in an average 28-day compressive strength of 39.5 MPa with a 1.6 MPa standard deviation. The reinforcement steel bars for all specimens were of Grade 500B as per BS 4449 standard [31]. Compression and transverse steel bars were 8 mm in diameter with a yielding stress of 298 MPa. The main reinforcing bars used were 10 mm and 16 mm in diameter with a yielding stress of 627 MPa and 594 MPa, respectively. The corresponding strains were 0.27% and 0.29%, respectively. The main steel reinforcement details are summarized in Table 1.

Table 1

Steel Reinforcement Properties

Bar type	Dia. 10 mm bar	Dia. 16 mm bar
Yield stress (MPa)	627	594
Yield strain ε_y (%)	0.27	0.29
Modulus of elasticity (GPa)	232	205

3.2 FRCM Properties

Three commercially available FRCM fabrics were utilized in this work, namely, Carbon (Ruredil X Mesh C10) [32], PBO (Ruredil X Mesh Gold) [33], and glass (Sikawrap-350G Grid) [34]. The different fabrics are all shown in Figure 2. The three The mechanical and geometric properties of each type are presented in Table 2. The associated mortars used in binding the FRCM layer to the concrete surface had 28-day compressive strengths of 30 ± 2.4 MPa, 20 ± 1.4 MPa, and 40 ± 2.3 MPa for Carbon-FRCM, PBO-FRCM, and Glass-FRCM, respectively, according to the tests performed in conformity with ASTM C109 [35]. Furthermore, FRCM characterization has been performed on 410 × 50 × 10 mm coupon tests in accordance with AC 434 [36]. The results of the FRCM coupon tests are summarized in Table 3.

(a) (b) (c)

Figure 2 FRCM fabrics: a) Carbon-FRCM, b) PBO-FRCM, c) Glass-FRCM

Table 2

Mechanical and Geometric Properties of FRCM Fabrics

Material	Spacing c/c (mm)	A_f (mm^2/ mm)	E (GPa)	F_{tu} (GPa)	ε_{ult}(%)
PBO	10	0.0455	270	5.8	2.15
Carbon	10	0.0470	240	4.8	1.80
Glass	18	0.0470	80	2.6	3.25

Table 3

FRCM Coupon Tests Results

FRCM	σ_{fu} (MPa)	ε_{fu} (%)	E_f (GPa)
PBO	1235	1.06	112
Carbon	1178	1.04	135
Glass	767	0.93	60

3.3 Test Matrix

In total, twenty (20) medium scaled RC beams were tested under four-point loading. The dimensions of the specimens were 2500 × 150 × 260 mm (length × width × height). The full test matrix is presented in Table 4. The specimens are designed with two different reinforcement ratios $\rho_s = 0.5\%$ and $\rho_s = 1.28\%$ representing deficient beams subjected to corrosion damage reducing the steel area and typical under-reinforced beams. The design details of the specimens are shown in Figure 3.

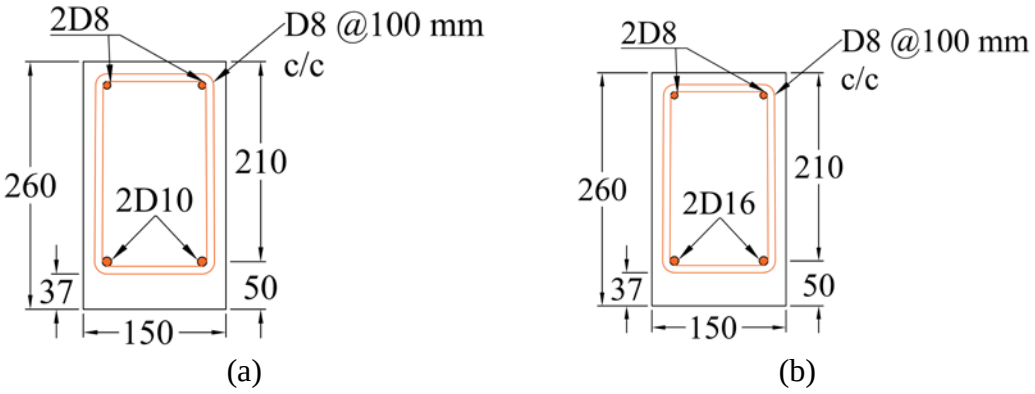

Figure 3 Reinforcement details (dimensions in mm): a) Beams with ρ_s=0.5%, b) Beams with ρ_s=1.28%

Two beams were kept un-strengthened as reference specimens. The remaining eighteen specimens were strengthened in flexure and divided into three main groups based on the strengthening scheme followed. Six beams were strengthened using the traditional EB-FRCM divided between the three FRCM systems (C-FRCM, P-FRCM, and G-FRCM) and two different reinforcement ratios ($\rho_s = 0.5\%$, and $\rho_s = 1.28\%$). Six beams were strengthened in NSE-FRCM divided between the three FRCM systems and the two reinforcement ratios. Similarly, six beams were strengthened using the hybrid NSE/EB FRCM. All EB and NSE strengthened specimens utilized two fabric plies within the FRCM layer while NSE/EB strengthened specimens used four fabric plies. The reference specimens are named in the "R-A" format where the R designated them as reference and A refers to the reinforcement ratio (L for $\rho_s = 0.5\%$, and H for $\rho_s = 1.28\%$). The strengthened specimens in Table 4 are named in the "X-Y-Z" format where X refers to the FRCM system utilized (P for PBO, C for Carbon, and G for Glass),

Y refers to the strengthening scheme (N for NSE, E for EB, and NE for the hybrid NSE/EB), and Z is the reinforcement ratio (L for $\rho_s = 0.5\%$, and H for $\rho_s = 1.28\%$).

The EB-FRCM was applied in the whole width of the beams while in the case of NSE-FRCM, it was only applied over 90 mm width. The hybrid NSE/EB-FRCM was applied on the beams in two parts, the internal 90 mm wide FRCM and the external 150 mm wide FRCM. The details of the strengthening are shown in Figure 4a through Figure 4c. The thickness of the FRCM layer is dependent on the FRCM system used where it is 10 mm for PBO-, and C-FRCM containing two plies of fabric. This value was 15 mm for G-FRCM also containing two fabric plies. This difference is due to the manufacturer's recommendations related to the different mortars used to allow proper bonding. In case of the hybrid NSE/EB strengthened beams, the total fabric plies are four (two are in the internal part and two are in the external part).

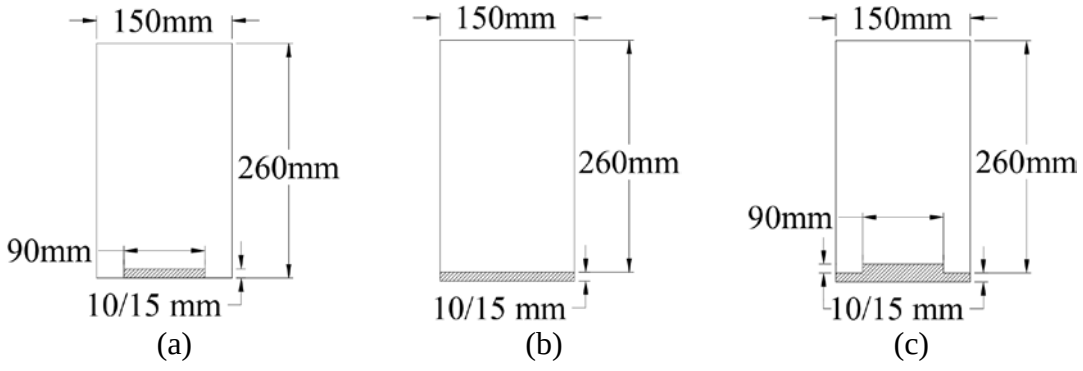

Figure 4 Strengthening details: a) Section of a NSE strengthened beam, b) Section of an EB strengthened beam, and c) A section of a NSE/EB strengthened beam

Table 4

Test Matrix

No.	ID	Fabric Type	Strengthening	Reinforcement ratio (%)
		Reference Specimens		
1	R-L	-	-	0.5
2	R-H	-	-	1.28
		Group 1 Specimens		
3	P-N-L	PBO	NSE	0.5
4	C-N-L	Carbon	NSE	0.5
5	G-N-L	Glass	NSE	0.5
6	P-N-H	PBO	NSE	1.28
7	C-N-H	Carbon	NSE	1.28
8	G-N-H	Glass	NSE	1.28
		Group 2 Specimens		
9	P-E-L	PBO	EB	0.5
10	C-E-L	Carbon	EB	0.5
11	G-E-L	Glass	EB	0.5
12	P-E-H	PBO	EB	1.28
13	C-E-H	Carbon	EB	1.28
14	G-E-H	Glass	EB	1.28
		Group 3 Specimens		
15	P-NE-L	PBO	NSE/EB	0.5
16	C-NE-L	Carbon	NSE/EB	0.5
17	G-NE-L	Glass	NSE/EB	0.5
18	P-NE-H	PBO	NSE/EB	1.28
19	C-NE-H	Carbon	NSE/EB	1.28
20	G-NE-H	Glass	NSE/EB	1.28

3.4 Preparation of Specimens

Steel cages have been prepared for all beams according to the design drawings. Prior to casting, strain gages have been installed on the main steel bars at midspan as shown in Figure 5.

Figure 5 Strain gages installed on main steel reinforcement

The formwork was prepared according to the designed beams dimensions and the steel cages were placed inside in preparation for casting as shown in Figure 6.

Figure 6 steel cages placed in formwork

The beams have then been cast and the surface finished as shown in Figure 7.

Figure 7 Concrete casting and finishing

The concrete specimens were then cured for a minimum of 28 days prior to the strengthening process.

3.4.1 NSE-FRCM Strengthened Beams

To strengthen the NSE strengthened specimens, the required area for the groove was first marked on the surface of the beam that is 90 mm wide throughout the length of the beam. A slitting machine has been used to cut the grooves on the surface of the beam as shown in Figure 8a. The grooves were 10 mm deep for PBO and Carbon strengthened beams, and 15 mm for Glass strengthened beams. In order to prepare the groove, multiple slits have been cut using the machine so that the next step becomes easier. The concrete between the slits then was chipped away manually using a chisel

and hammer as shown in Figure 8b. The surface was then cleaned from debris resulting in the rough surface shown in Figure 8c.

(a)

(b)

(c)

Figure 8 NSE beams preparation: a) Using slitting machine to cut the grooves, b) Manually chipping away the cut concrete, and c) Finished surface after cleaning

After the concrete surface preparation, the surface was then saturated with water for 30 mins to prepare for the strengthening material. First, the mortar was mixed with water according to the specifications of each specific mortar type. Then, a thin layer of mortar was applied in the groove completely covering the roughened surface shown in Figure 9a. One layer of fabric was then placed on the mortar as shown in Figure 9b. and pressed manually to ensure complete impregnation as shown in Figure 9c. Another layer of mortar was then placed on top and the process repeated with the second fabric layer. Finally, a final layer of mortar was placed on top and the surface finished to flush with the original concrete surface shown in Figure 9d.

Figure 9 NSE-FRCM application: a) applying the first layer of mortar, b) placing the first layer of fabric, c) impregnation of fabric, and d) finished surface for NSE beams

3.4.2 EB-FRCM Strengthened Beams

The surface preparation for the EB strengthened beams was done using sandblasting over the whole length and width of the beam to ensure good contact between FRCM and concrete substrate surface. The FRCM was applied similarly to the

NSE strengthened specimens where the first layer of mortar was applied. The FRCM layer was then placed and manually pressed to ensure full impregnation. The process was repeated for the second layer. A final layer of mortar was then applied and the surface finished.

3.4.3 Hybrid NSE/EB-FRCM Strengthened Beams

The preparation for the hybrid specimens was a combination between grooving and sandblasting where the internal part was grooved and chipped manually and the external part was sandblasted as shown in Figure 10.

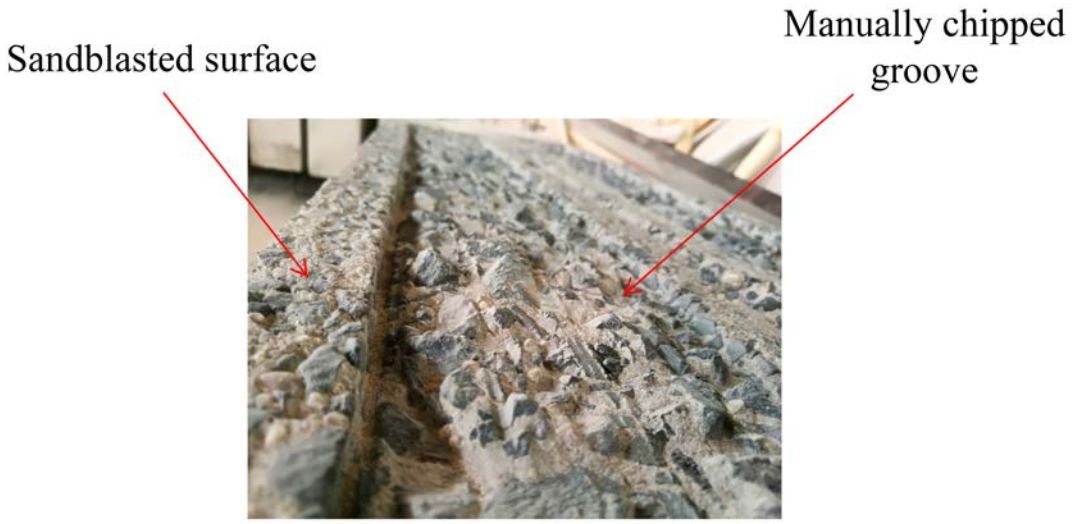

Figure 10 Hybrid specimens roughened surface

The FRCM layer was applied similar to the rest but with a total of four layers of fabric. A thin layer of mortar was first applied on the surface of the groove and the first fabric layer manually impregnated in it as shown in Figure 11a. The process was repeated for

the second internal fabric layer but the surface was not finished after that. A 4-5 mm layer of mortar was then applied to completely cover the groove and act as the first layer of mortar for the outer part as shown in Figure 11b. Then the first fabric layer was applied and impregnated into the mortar layer as shown in Figure 11c. The process was repeated for the second outer fabric layer and the surface finished as shown in Figure 11c after applying the final mortar layer.

(a)

(b)

(d)

(e)

Figure 11 Hybrid NSE/EB specimens strengthening: a) Impregnating first internal fabric layer, b) applying mortar on top of internal layers, c) impregnating first outer fabric layer, and d) finished surface

3.5 Test setup and instrumentation

The specimens were tested under four-point loading as shown in Figure 12a. The loading rate was 1 mm/min until failure. Two linear variable displacement transducers (LVDTs) were placed at midspan to measure midspan deflection during loading. One strain gage was installed on the top surface of the specimens to measure concrete strain. The installed LVDTs and strain gage are shown in Figure 12b.

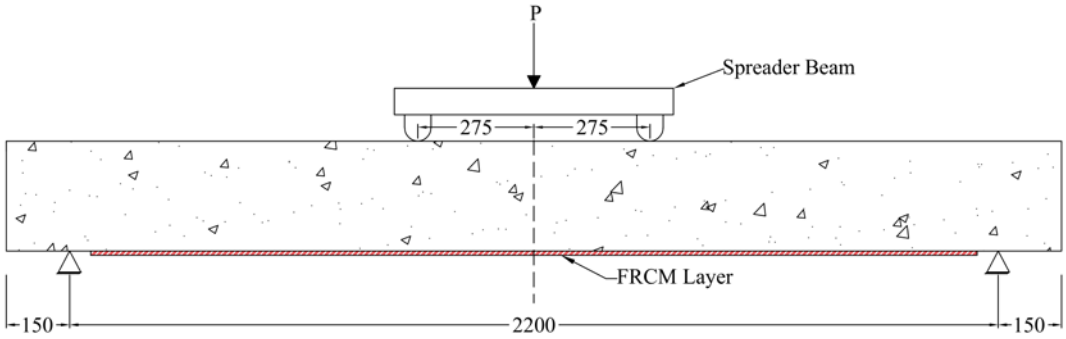

(a)

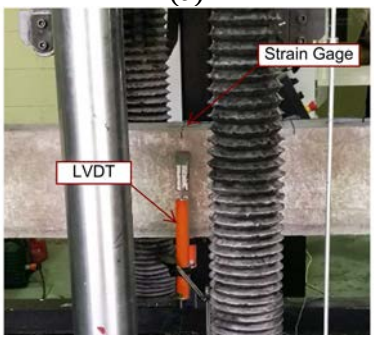

(b)

Figure 12 Test setup and instrumentation (dimensions in mm)

A picture of a specimen placed in the machine during testing is shown in Figure 13 for Specimen C-N-H.

Figure 13 Specimen C-N-H during testing

The strain gages used for data collection during testing are detailed in Table 5. A total of two steel strain gages on the main reinforcement steel and one concrete strain gage were installed. The concrete strain gage was installed on the top of the section at midspan to measure compression strains.

Table 5

Strain Gages Details

Material application	Concrete	Steel
Gage type	PL-60-11	FLA-5-11
Gage length (mm)	60	5
Gage factor	2.13	2.13
Strain limit	2% (20,000 $\mu\varepsilon$)	5% (50,000 $\mu\varepsilon$)
Resistance (Ω)	120	120

The data for the strain gages (steel and concrete) and LVDTs were collected at a rate of 1 Hz using a data acquisition system, TML datalogger, shown in Figure 14.

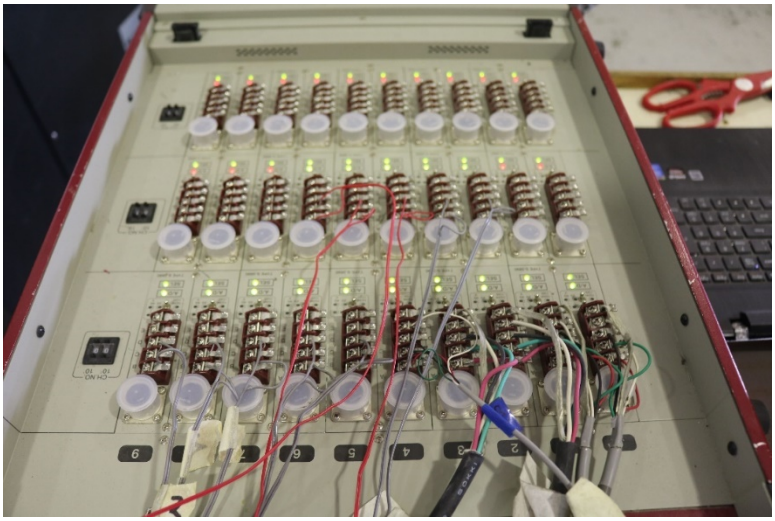

Figure 14 TML data logger

CHAPTER 4: RESULTS AND DISCUSSION

4.1 Results

In this chapter, the results are shown and analyzed. The analysis is done in terms of the ultimate load carrying capacity, deformational characteristics (Stiffness and ductility), and modes of failure. A summary of the test results for all the tested specimens is presented in Table 6. The results are presented in terms of axial stiffness factor (κ^f), stiffness factor (β^f), ultimate load carrying capacity (P_u), gain in P_u, initial stiffness (S_I), post-cracking stiffness (S_c), deflection at ultimate load (δ_u), ductility index (ΔI), concrete compressive strain at ultimate load (ε_{cu}), and failure modes. The failure modes are represented by the notations SY (steel yielding), CC (concrete crushing), M-S (midspan delamination), FR (fabric rupture), and D-PE (plate-end delamination)

4.1.1 Equivalent Stiffness Factor

The equivalent axial stiffness, κ^f, and stiffness factor, β^f, are calculated for all specimens so that aa direct comparison between different strengthening schemes is possible. The FRCM width in NSE strengthened specimens is 90 mm while that value is 150 mm for EB strengthened specimens and the hybrid specimens have both widths, thus necessitating the use of these factors. The equivalent axial stiffness factor, κ^f, is a quantifiable measure that incorporated both the cracked modulus of elasticity and effective cross-sectional area of the FRCM fabric and evaluated as follows [14]:

$$k^f = \frac{nA_f b_f E_f}{(bd_f)} = \rho_f E_f \quad (1)$$

Where n = number of fabric plies, A_f= Equivalent area of fabric per unit width shown in Table 2, E_f = cracked modulus of elasticity of FRCM listed in Table 3, b_f = fabric width (90 mm for NSE, 150 mm for EB, both 90 mm and 150 mm for NSE/EB), d_f= FRCM depth from the top of the specimen cross-section (255 for NSE, 265 for EB,

and 261.25 for NSE/EB), b= width of beam section (150 mm), and ρ_f=fabric reinforcement ratio listed in Table 6 and calculated as follows:

$$\rho_f = \frac{nA_f b_f}{bd_f} \quad (2)$$

The ratio of the contribution of FRCM composites to strengthening to that of steel reinforcement is expressed as the stiffness factor, β^f, incorporating the volume fraction of fabric and the steel reinforcement and calculated as follows [14]:

$$\beta^{\mathrm{f}} = \frac{k^f}{\rho_{\mathrm{s}} \mathrm{E}_{\mathrm{s}}} \quad (3)$$

Where ρ_s= steel reinforcement ratio (0.5% for low reinforcement and 1.28% for high reinforcement). The values of κ^f and β^f as calculated for all specimens and listed in Table 6.

Table 6

Summary of Test Results

Specimen	ρ_s (%)	ρ_f (%)	κ^f (MPa)	β^f	P_u (kN)	P_u gain (%)	S_I (kN/mm)	S_c (kN/mm)	δ_u (mm)	ΔI	ε_{cu} ($\mu\varepsilon$)	Failure Mode
Reference Specimens												
R-L	0.5	-	-	-	39.9	-	15.1	3.53	27.2	15.31	3640	SY + CC
R-H	1.28	-	-	-	99.2	-	26.8	7.85	24.7	7.31	3760	SY + CC
Group 1												
P-N-L	0.5	0.021	24	2.53	62.7	57.1	26.8	7.85	28.1	5.73	2805	M-S
C-N-L	0.5	0.022	29.9	3.15	59.2	48.4	26.5	5.03	16.1	3.21	1076	M-S
G-N-L	0.5	0.022	13.3	1.4	52.4	31.4	16.2	4.11	22.9	5.56	2717	FR
P-N-H	1.28	0.021	24	0.99	123	83.5	22.9	9.42	26.2	3.6	2682	M-S
C-N-H	1.28	0.022	29.9	1.23	124	84.3	23.7	9.74	17.5	2.45	2457	M-S
G-N-H	1.28	0.022	13.3	0.55	110	70.4	25.2	8.79	21.0	2.87	2513	FR
Group 2												
P-E-L	0.5	0.034	38.5	4.06	68.9	72.8	31.3	4.92	25.7	4.53	2027	D-PE
C-E-L	0.5	0.035	47.9	5.06	68.7	72.2	26.8	5.05	16.1	3.04	1507	M-S
G-E-L	0.5	0.035	21.3	2.25	51.9	30.1	30.5	4.17	13.1	3.03	1495	FR
P-E-H	1.27	0.034	38.5	1.59	131	92.2	43.2	10.15	20.0	2.78	2144	M-S
C-E-H	1.27	0.035	47.9	1.97	132	93.3	29.2	9.58	21.2	2.05	2871	M-S
G-E-H	1.27	0.035	21.3	0.88	113	73.5	28.6	7.35	21.2	2.93	2794	FR
Group 3												
P-NE-L	1.28	0.056	62.4	6.59	82.7	107.3	16.8	5.5	29.7	5.55	2625	D-PE
C-NE-L	1.28	0.058	77.7	8.21	83.2	108.6	42.2	5.9	21.6	3.96	1850	M-S
G-NE-L	1.28	0.058	34.5	3.65	58.2	45.8	30.1	4.1	17.9	3.67	1461	FR
P-NE-H	0.00	0.056	62.4	2.57	136	96.8	27.4	9.3	20.2	2.45	2603	D-PE
C-NE-H	0.00	0.058	77.7	3.21	144	104.7	21.1	10.1	20.5	2.70	2352	M-S
G-NE-H	0.00	0.058	34.5	1.42	124	84.5	30.8	9.8	17.1	2.35	2126	FR

4.1.2 Load-Deflection Relationships

From the load-deflection relationships, the initial stiffness (S_I) and post-cracking stiffness (S_c) values are evaluated. The initial stiffness, S_I, is defined as the slope of the load-deflection curve up to the initial crack while the post-cracking stiffness, S_c, is defined as the slope of the load-deflection curve after the initial crack and before reaching the yield load. The evaluation of both S_I and S_c values is shown in Figure 15. The load-deflection relationships for all tested specimens are shown in Figure 16 for Group 1 specimens, Figure 17 for Group 2 specimens, and Figure 18 for Group 3 specimens. Each figure displays the different FRCM system used per reinforcement ratio (ρ_s=0.5%, and ρ_s= 1.28%) and strengthening scheme (NSE, EB, and NSE/EB) in reference to the corresponding control specimen.

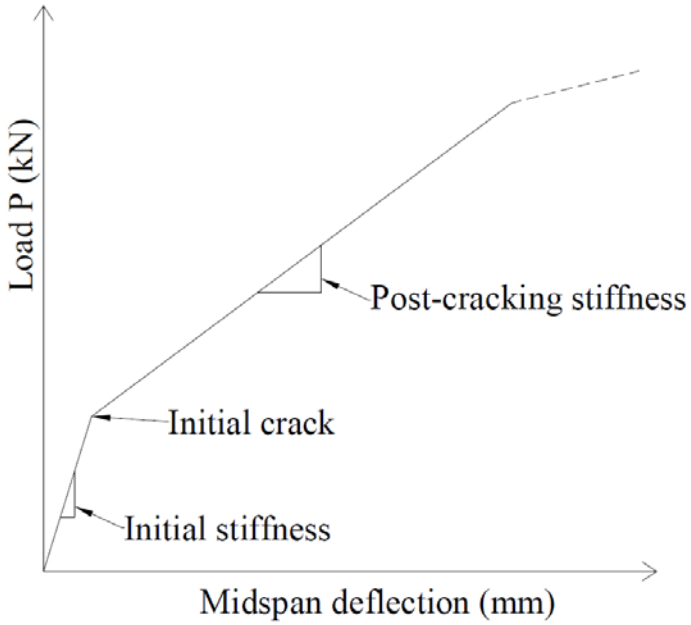

Figure 15 Initial and post-cracking stiffness values evaluation

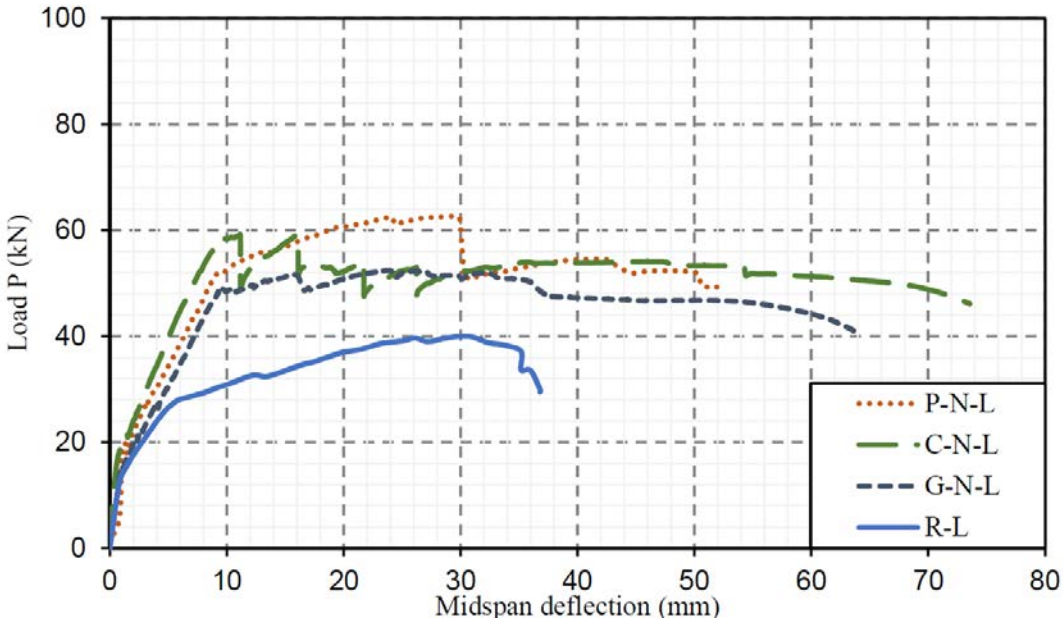

(a)

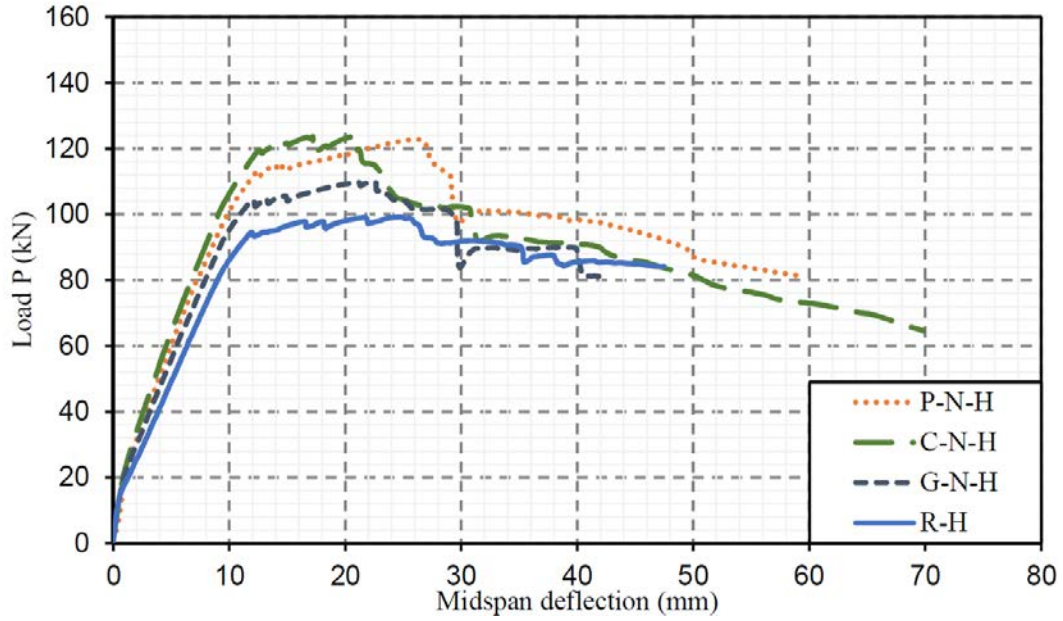

(b)

Figure 16 Load-deflection relationships for Group 1 specimens: a) low reinforcement, and b) high reinforcement

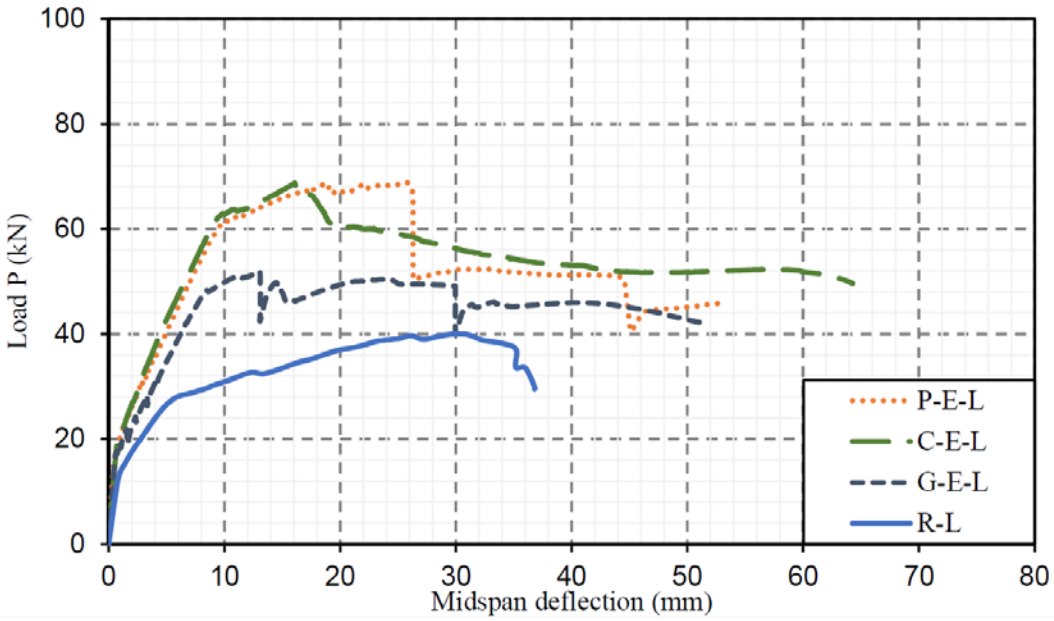

(a)

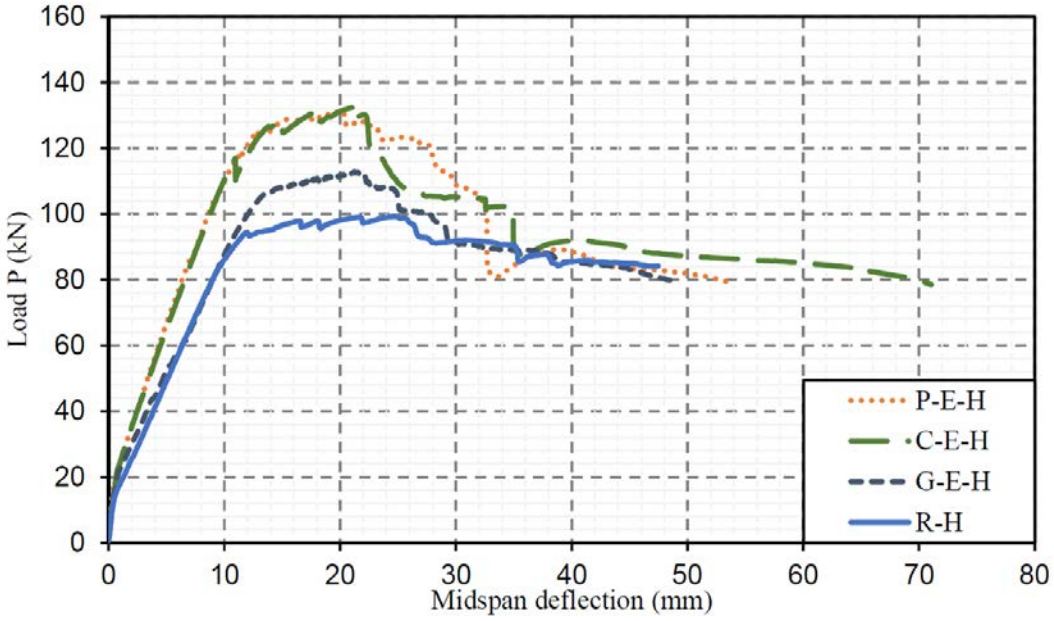

(b)

Figure 17 Load-deflection relationships for Group 2 specimens: a) low reinforcement, and b) high reinforcement

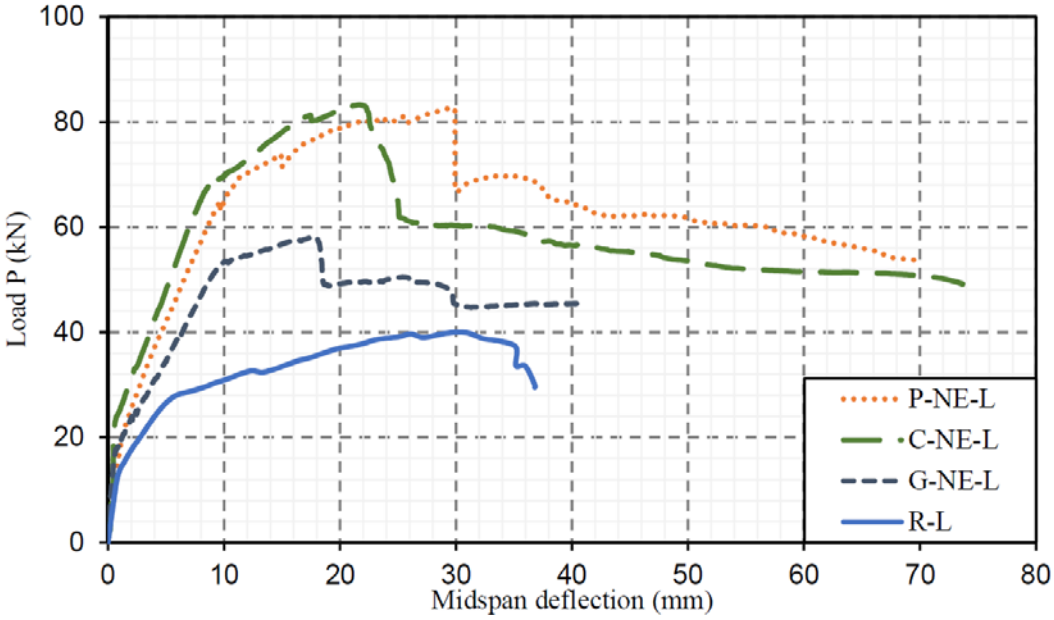

(a)

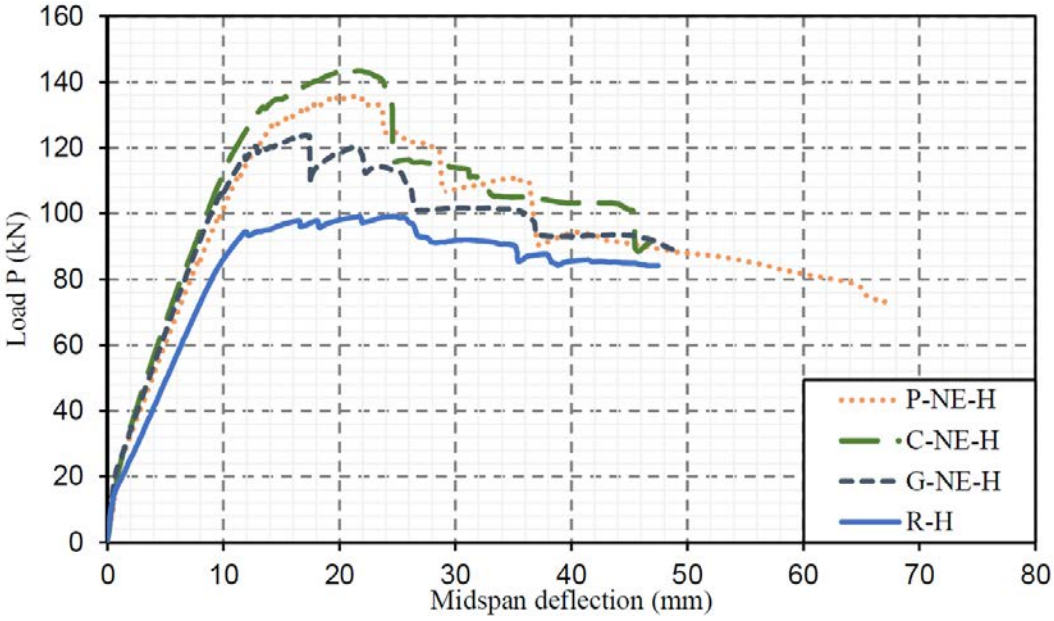

(b)

Figure 18 Load-deflection relationships for Group 3 specimens: a) low reinforcement, and b) high reinforcement

4.2 Discussion

4.2.1 Load Carrying Capacity

Significant gains in P_u were observed for all strengthened specimens with Group 1 specimens having gain in P_u values ranging from 57.1% for Specimen P-N-L to 84.3% for Specimen C-N-H. The values for the gain in P_u for Group 2 Specimens ranged between 30.1% for Specimen G-E-L and 93.3% for Specimen G-E-H. As for Group 3 specimens, the P_u gain ranged between 45.8% for Specimen G-NE-L and 108.6% for Specimen C-NE-L. Analyzing the effect of the reinforcement ratio reveals that the strengthening effect is more noticeable for specimens with lower reinforcement ratio ($\rho_s = 0.5\%$) compared to those of higher reinforcement ratio ($\rho_s = 1.28\%$) except with Group 3 Specimens. Beams with $\rho_s = 0.5\%$ for Group 1 (P-N-L, C-N-L, and G-N-L) and Group 2 (P-E-L, C-E-L, and G-E-L) had an average P_u gain of 45.6% and 58.4%, respectively, compared to the control specimen R-L. This value was 87.2% for Group 3 specimens (P-NE-L, C-NE-L, and G-NE-L). As to specimens with $\rho_s = 1.28\%$, the average P_u gain was 79.4% and 86.3% for Group 1 specimens (P-N-H, C-N-H, and G-N-H) and Group 2 specimens (P-E-H, C-E-H, and G-E-H), respectively, when compared with the control specimen R-H. The value was 95.3% for group 3 specimens (P-NE-H, C-NE-H, and G-NE-H).

Regarding the fabric type, the results are assessed based on the different fabric types used (PBO, Carbon, and Glass). The average P_u gain for PBO-FRCM strengthened specimens (P-N-L, P-N-H, P-E-L, P-E-H, P-NE-L, and P-NE-H) was 84.9% compared to their respective control specimens which is close to that of Carbon-FRCM strengthened specimens (C-N-L, C-N-H, C-E-L, C-E-H, C-NE-L, and C-NE-H) which was 85.3%. That value was 56% for Glass-FRCM strengthened specimens (G-N-L, G-N-H, G-E-L, G-E-H, G-NE-L, and G-NE-H) which is lower than the other

fabric types. This indicates similar strengthening gains for PBO- and Carbon-FRCM with very close average P_u gain values with lower gains from Glass-FRCM.

Comparing the different strengthening schemes (NSE, EB, and NSE/EB) shows favorable results for both NSE strengthening and NSE/EB strengthening compared to EB strengthening. The average gain in P_u values were 62.5%, 72.3%, and 91.3%, for Group1, Group 2, and Group 3 specimens, respectively. The values for Group 1 and Group 2 indicate comparable performance while Group 1 specimens use only 60% of the FRCM composite compared to Group 2 specimens while Group 3 specimens shows the best gains in P_u due to strengthening. To further clarify the comparison, the values of P_u gain and β^f are plotted in Figure 19 where data points closer to the top right corners show increased FRCM utilization. The comparison shows that the best FRCM utilization is present in Group 3 specimens, where the points are closer to the higher end of the trend lines compared to their Group 1 and Group 2 counterparts.

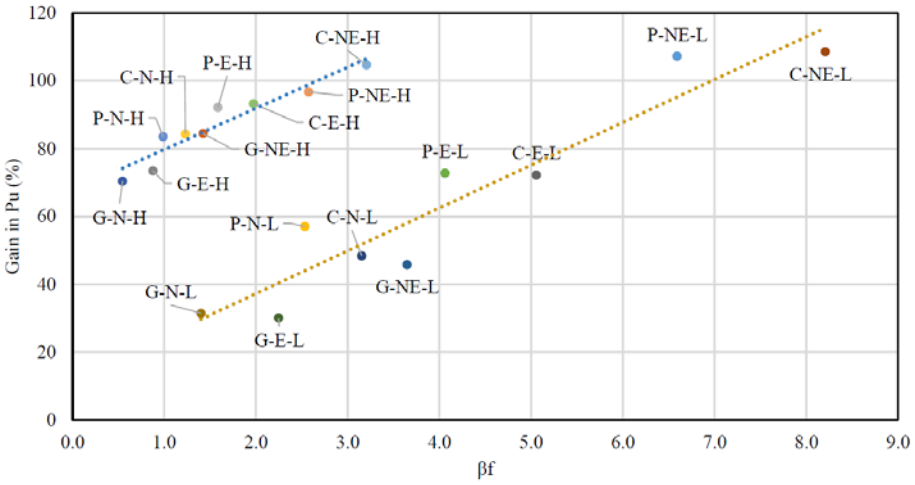

Figure 19 Gain in P_u vs β^f

These comparisons show that NSE strengthening has improved bonding between FRCM and concrete substrate compared to the traditional EB strengthening. The hybrid NSE/EB strengthening offers the best results in terms of load carrying capacity and stiffness which is in line with Wakjira's work on shear strengthening [13,37].

4.2.2 Deformational Characteristics

4.2.2.1 Initial and post-cracking stiffness

The initial, S_I, and post-cracking stiffness, S_c, values are here analyzed to investigate the effect of the different reinforcement ratios, strengthening schemes. The average S_I value for the reference specimens was 21 kN/mm. This value was increased due to strengthening to 23.6 kN/mm, 31.6 kN/mm, and 28.1 kN/mm for Group 1, Group 2, and Group 3 specimens respectively. The lower S_I value for Group 1 specimens is attributed to the reduced height of the strengthened specimens (260 mm) compared to that of Group 2 and Group 3 specimens (270/275 mm) since increasing the beam height increases the uncracked moment of inertia that in turn reduces deflection and increases initial stiffness of uncracked section. Both EB and NSE/EB strengthening schemes offer close initial stiffness values since in the uncracked stage of loading, the FRCM is not yet utilized. While the S_I values are scattered and do not offer a clear trend, the average values however offer insight into the performance of these specimens. The average S_I for group 1 specimens was very close to that of the reference specimens while that value for beams with $\rho_s = 0.5\%$ (P-N-L, C-N-L, and G-N-L) was 31.2 kN/mm compared to 15.1 kN/mm for reference R-L. Beams with $\rho_s = 0.5\%$ in Group 2 (P-E-L, C-E-L, and G-E-L) and Group 3 (P-NE-L, C-NE-L, and G-NE-L) have very close average S_I values of 29.5 kN/mm and 29.7 kN/mm, respectively, which is close to that of Group 1 indicating similar initial stiffness increase for EB and NSE/EB strengthening of flexure deficient beams. The average S_I values for specimens with

$\rho_s = 1.28\%$ were 23.9 kN/mm, 33.7 kN/mm, and 26.4 kN/mm for Group 1 (P-N-H, C-N-H, and G-N-H), Group 2 (P-E-H, C-E-H, and G-E-H), and Group 3 (P-NE-H, C-NE-H, and G-NE-H) specimens, respectively, showing that EB strengthening offers the highest S_I increase with high reinforcement ratios.

Analyzing the post-cracking stiffness, S_c, values show different behavior compared to the initial stiffness. The average S_c values for Group 1, Group 2, and Group 3 specimens were 7.5 kN/mm, 6.9 kN/mm, and 7.4 kN/mm, respectively. This indicates that the EB strengthening offers the lowest increase in post-cracking stiffness of the section compared to the NSE and NSE/EB counterparts, which on average, provide similar increase in S_c. The average S_c values for beams with $\rho_s = 0.5\%$ were 5.7 kN/mm, 4.7 kN/mm, and 5.2 kN/mm for Group 1 (P-N-L, C-N-L, and G-N-L), Group 2 (P-E-L, C-E-L, and G-E-L), and Group 3 (P-NE-L, C-NE-L, and G-NE-L) specimens, respectively. These values were 9.3 kN/mm, 9.0 kN/mm, and 9.7 kN/mm for specimens with $\rho_s = 1.28\ \%$ from Group 1 (P-N-H, C-N-H, and G-N-H), Group 2 (P-E-H, C-E-H, and G-E-H), and Group 3 (P-NE-H, C-NE-H, and G-NE-H), respectively. This indicates that higher reinforced specimens are more affected in general in terms of post-cracking stiffness with the NSE/EB strengthening offering the highest increase and EB strengthening offering the lowest.

4.2.2.2 Ductility

There was a general decrease in the ductility index, ΔI, due to the strengthening with the average ΔI values being 3.9, 3.06, and 3.45 for Group 1, Group 2, and Group 3 specimens, respectively, compared to the average ΔI of 11.31 of the control specimens. It is however observed that the EB strengthening offers the lowest average ΔI value compared to the NSE strengthening which was the highest and the NSE/EB being in between. This indicates that NSE strengthening and the NSE part of the hybrid

NSE/EB strengthening lead to limited debonding/delamination possibilities. Checking the reinforcement effect shows that flexure deficient beams have increased ΔI values compared to their under reinforced counterparts. The average ΔI values for specimens with $\rho_s = 0.5\%$ were 4.8, 3.5, and 4.4 for Group 1 (P-N-L, C-N-L, and G-N-L), Group 2 (P-E-L, C-E-L, and G-E-L), and Group 3 (P-NE-L, C-NE-L, and G-NE-L) specimens, respectively. These values were 3.0, 2.6, and 2.5 for specimens with $\rho_s = 1.28\ \%$ from Group 1 (P-N-H, C-N-H, and G-N-H), Group 2 (P-E-H, C-E-H, and G-E-H), and Group 3 (P-NE-H, C-NE-H, and G-NE-H), respectively.

4.2.3 Failure Modes and Cracking Patterns

All failure modes observed on all specimens are summarized in Table 6. The schematic drawings of the reference beams R-L and R-H are shown in Figure 20a and Figure 20b, respectively. Bothe control specimens failed due to steel yielding followed by concrete crushing with large flexural cracks forming at mid-section. Group 1, Group 2, and Group 3 specimens cracking patterns are shown in Figure 21a through Figure 21f, Figure 22a through Figure 22f, and Figure 23a through Figure 23f, respectively. All specimens exhibited large flexural cracks forming at mid-span. After reaching ultimate loads, most specimens exhibited concrete crushing at mid-span until ultimate failure.

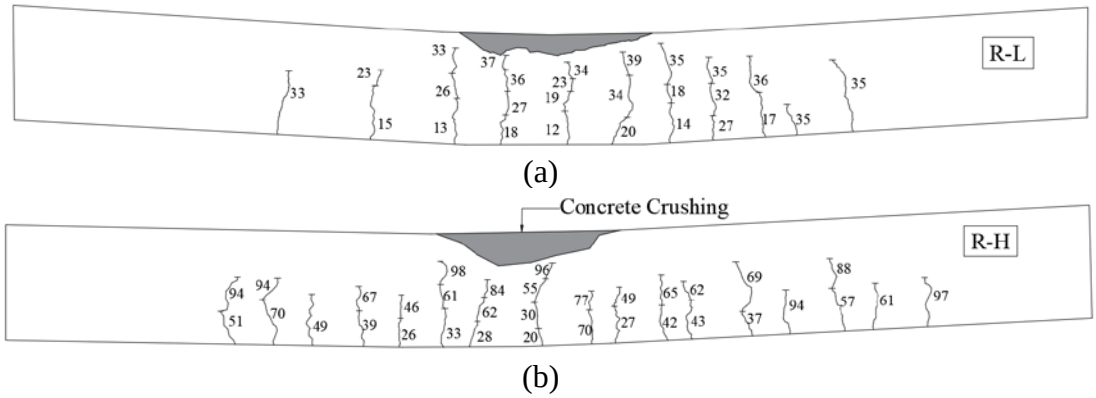

(a)

(b)

Figure 20 Reference specimens cracking patterns: a) R-L, and b) R-H

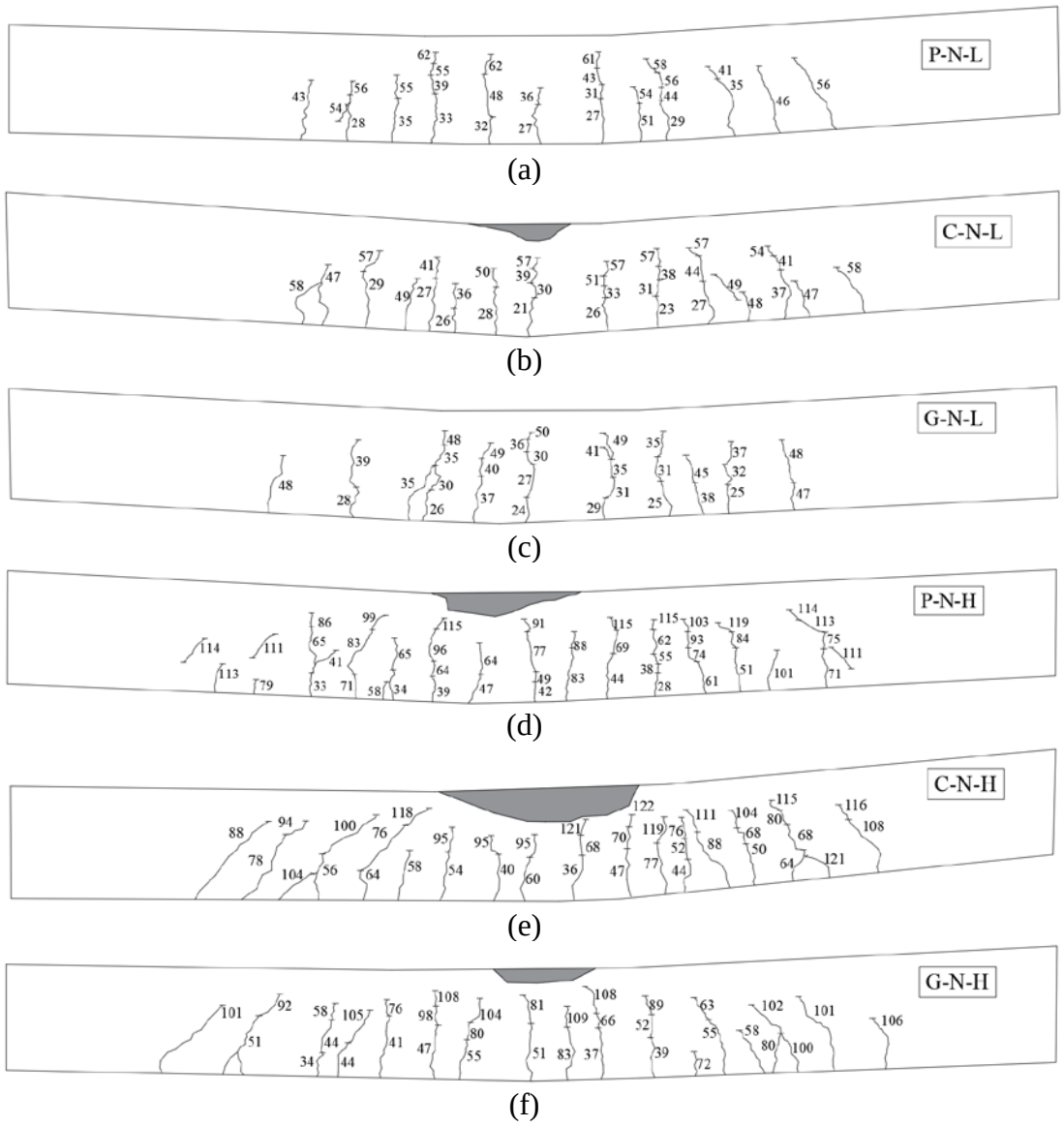

Figure 21 Group 1 Specimens cracking patterns: a) P-N-L, b) C-N-L, c) G-N-L, d) P-N-H, e) C-N-H, and f) G-N-H

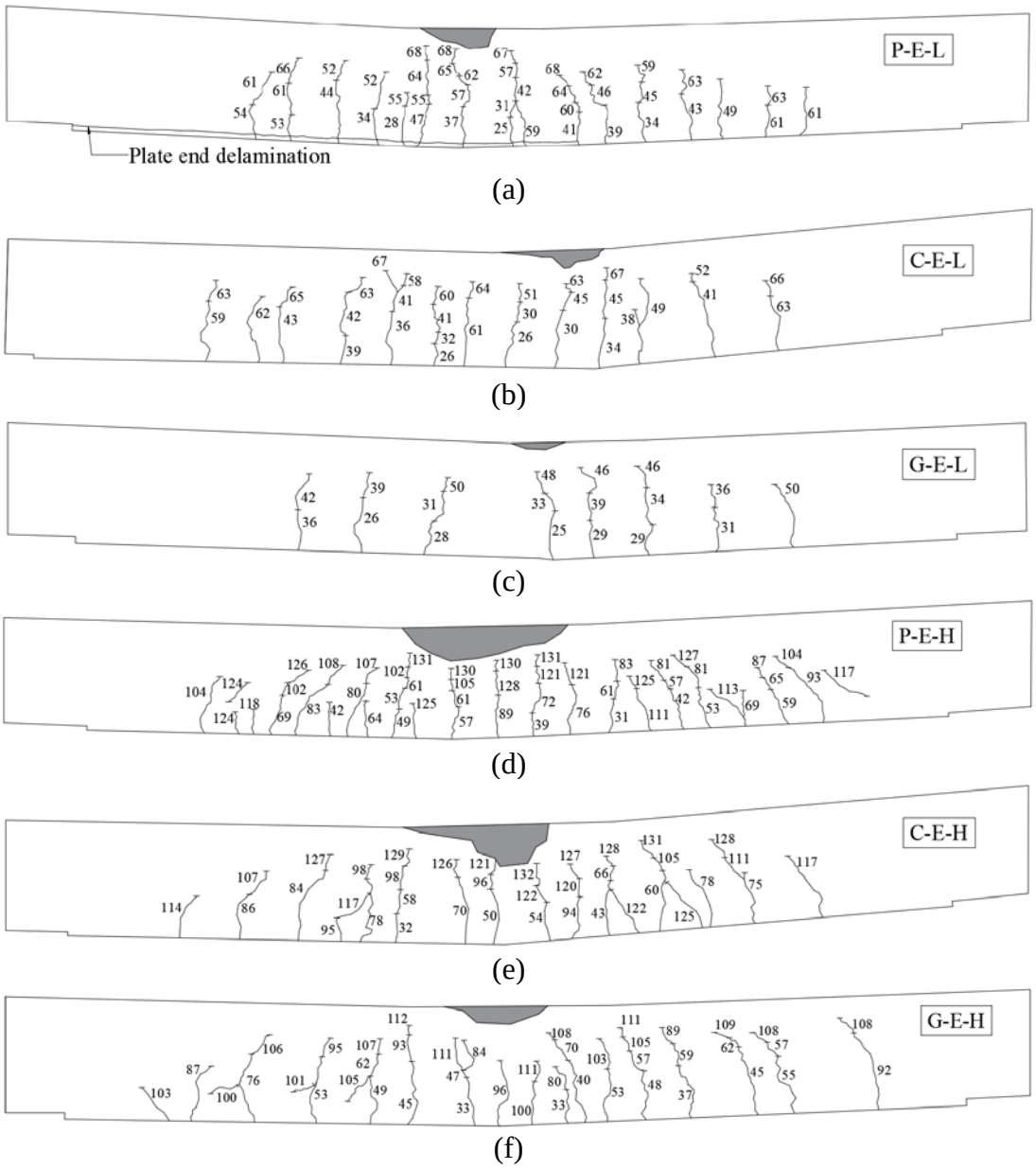

Figure 22 Group 2 Specimens cracking patterns: a) P-E-L, b) C-E-L, c) G-E-L, d) P-E-H, e) C-E-H, and f) G-E-H

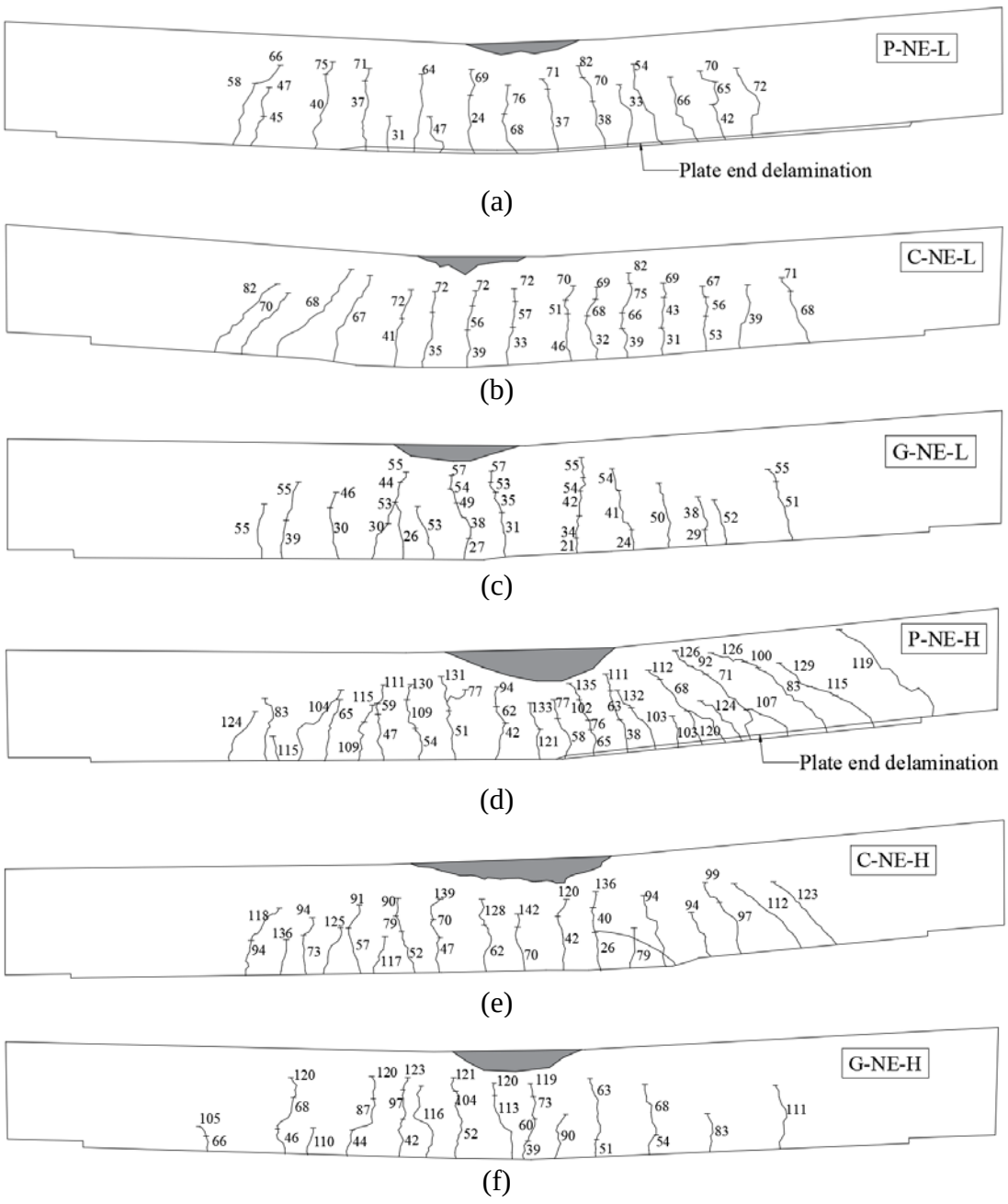

Figure 23 Group 3 Specimens cracking patterns: a) P-NE-L, b) C-NE-L, c) G-NE-L, d) P-NE-H, e) C-NE-H, and f) G-NE-H

The exhibited failure modes of strengthened specimens can be categorized as follows:

1) Large flexural cracks originating at mid-span: This was typical and was observed on all unstrengthened and strengthened specimens regardless of group as shown in the cracking patterns figures.
2) Mid-span FRCM delamination: In this mode of failure, the fabrics caused separation from the surrounding mortar matrix at mid-span after elongating. The FRCM layer at the ends was still bonded to the concrete substrate however. This mode of failure was exhibited by all C-FRCM strengthened specimens in Group 1 (C-N-L, and C-N-H), Group 2 (C-E-L, and C-E-H), and Group 3 (C-NE-L, and C-NE-H). This was also exhibited by PBO-FRCM strengthened specimens in Group 1 (P-N-L, and P-N-H) and specimen P-E-H of Group 2 indicating an advantage in favor of NSE strengthening over EB strengthening since specimen P-N-L did not fail due to debonding like its Group 2 counterpart. This mode of failure indicates that the strengthening system has been effective in avoiding plate end debonding, however, allowing the specimens to fail due to delamination at mid-span that occurred at higher loads than those which failed die to plate-end debonding. Figure 24b shows a close-up of this mode of failure in specimen C-NE-L.
3) Plate end FRCM delamination: This mode of failure was exhibited in specimen P-E-L of Group 2 and the external part of specimens P-NE-L, and P-NE-H of Group 3, were the FRCM layer was split at the composite end at the fabric level.. A close up of this mode of failure is shown in Figure 24c for specimen P-NE-H. The cracking patterns for specimens P-E-L, P-NE-L, and P-NE-H are shown in Figure 22a, Figure 23a, and Figure 23d, respectively, showing large cracks along the FRCM layer starting at mid-span and propagating to the plate ends

resulting in complete separation between fabric and matrix as shown in Figure 24c. This failure mode is only exhibited in PBO-FRCM strengthened specimens due to the high stiffness of the PBO fabric mesh. It was avoided in specimens P-N-L and P-N-H in Group 1 due to the improved bond between FRCM and concrete substrate.

4) FRCM fabric rupture: This mode of failure was exhibited by all G-FRCM strengthened specimens of all groups. This is similar to the results obtained from shear bond tests [15] and consistent with other flexure tests on FRCM strengthened RC beams [8,20]. This mode was exhibited due to the low stiffness of the glass fabric.

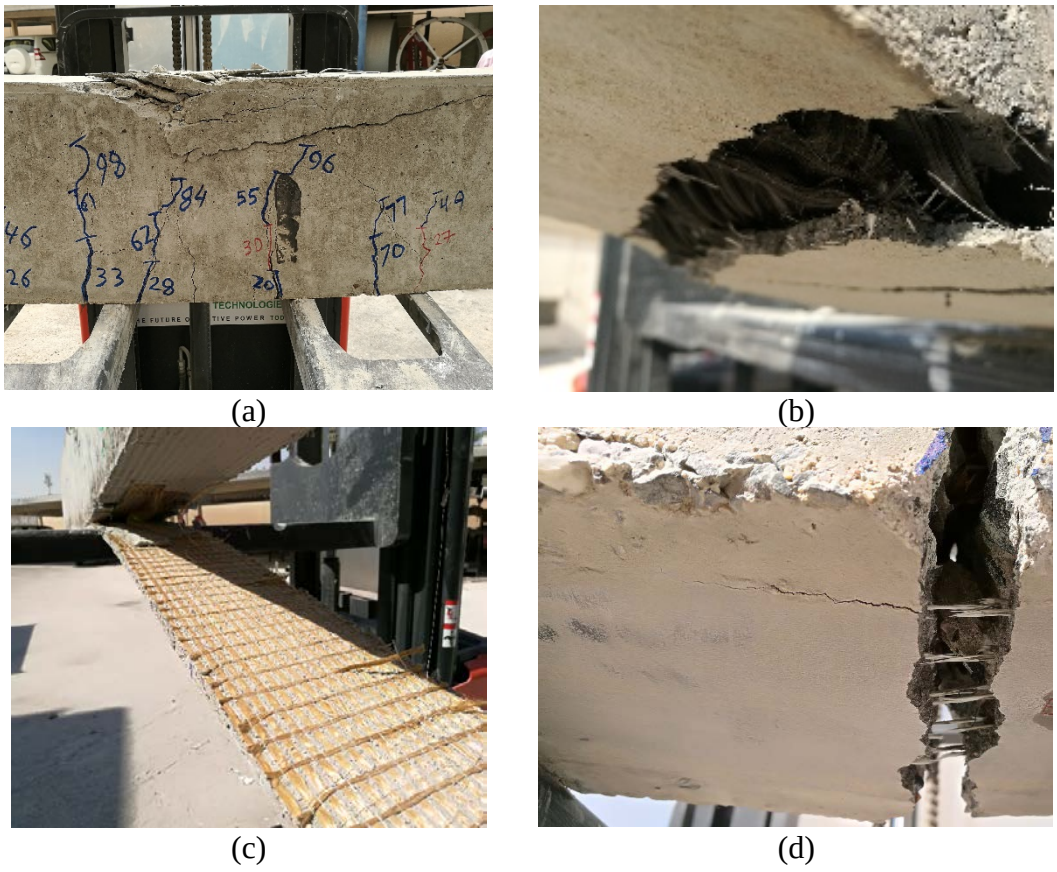

Figure 24 Failure modes: a) steel yielding (R-H), b) mid-span fabric delamination (C-NE-L), c) FRCM end plate debonding (P-NE-H), and d) fabric rupture (G-N-L)

CHAPTER 5: THEORETICAL CALCULATIONS

The ultimate load carrying capacities, P_u, obtained experimentally were compared with the theoretical formulation from ACI 318 and ACI 549 [24,38]. The analysis is based on the following assumptions:

- Plane sections remain plain after loading.
- Perfect bond between FRCM and the concrete substrate.
- Ultimate compressive strain in concrete is 0.003.
- Steel reinforcement is assumed to behave elastic-perfectly plastic.
- FRCM follows a bilinear behaviour where the behaviour is linear elastic up to failure and the post-cracking stiffness is taken into account. The E_f values used are shown in Table 3 from tensile coupon tests.

Based on ACI 549, the effective FRCM composite tensile strain at failure is limited by Eq (4):

$$\varepsilon_{fe} = \varepsilon_{fu} \leq 0.012 \tag{4}$$

Where ε_{fu} = FRCM ultimate tensile strain from coupon test. The effective stress level in the FRCM composite is calculate in accordance with Eq (5):

$$f_{fe} = E_f \varepsilon_{fe} \text{ where } \varepsilon_{fe} \leq \varepsilon_{fd} \tag{5}$$

Effective concrete strain (ε_c), and steel reinforcement strains (ε_t and ε_s') are computed as shown in Eq (6) in accordance with strain compatibility:

$$\frac{\varepsilon_{fe}}{d_f - c_u} = \frac{\varepsilon_t}{d - c_u} = \frac{\varepsilon_s'}{c_u - d'} = \frac{\varepsilon_c}{c_u} \tag{6}$$

Where d = distance from top of the beam to the main steel reinforcement, d_f = distance from top of the beam to the centre of the FRCM reinforcement, d' = distance from top of the beam to the top steel reinforcement. And c_u = neutral axis depth from the top. Internal forces equilibrium is satisfied as given by Eqs (7.1 through 7.4):

$$T_s + T_f = C \tag{7.1}$$

$$T_s = A_s f_y - A'_s E_s \varepsilon'_s \tag{7.2}$$

$$T_f = n A_f b_f E_f \varepsilon_{fe} \tag{7.3}$$

$$C = \alpha_1 f'_c \beta_1 c_u b \tag{7.4}$$

Where T_s = tension force in steel reinforcement, T_f = tension force in FRCM reinforcement, C = compression force in the concrete, A_S = cross-sectional area of main steel reinforcement, A'_s = cross-sectional area of top steel reinforcement, and ε'_s = strain in top steel reinforcement. The stress block parameters α_1 and β_1 are calculated in accordance with ACI 318 as shown in Eqs (8.1 and 8.2):

$$\beta_1 = \frac{4\varepsilon'_c - \varepsilon_c}{6\varepsilon'_c - 2\varepsilon_c} \tag{8.1}$$

$$\alpha_1 = \frac{3\varepsilon'_c \varepsilon_c - \varepsilon_c^2}{3\beta_1 {\varepsilon'_c}^2} \tag{8.2}$$

Where ε'_c is defined as follows in Eq 9:

$$\varepsilon'_c = 1.7 \frac{f'_c}{E_c} \tag{9}$$

The ultimate flexural moment M_u of the beam is then calculated according to Eqs (10.1 through 10.3):

$$M_u = M_s + M_f \tag{10.1}$$

$$M_s = A_s f_y \left(d - \frac{\beta_1 c_u}{2}\right) + A'_s E_s \varepsilon'_s (d - d') \tag{10.2}$$

$$M_f = T_f \left(d_f - \frac{\beta_1 c_u}{2}\right) \tag{10.3}$$

Where M_s = moment contribution of steel reinforcement, and M_f = moment contribution of FRCM reinforcement. The theoretical ultimate load carrying capacity P_{u-th} is then calculated as follows in Eq. 10:

$$P_{u-th} = \frac{2M_u}{l} \quad (10)$$

Where l = shear span of the loaded beam (825 mm). The calculated P_{u-th} values for all specimens are listed in Table 7. An example calculation is shown for G-E-L in the appendix.

There was a reasonable agreement between the theoretical and experimental values of the load carrying capacity for most of the specimens with the calculated theoretical values being underpredicted. The average error values were 13%, 10%, and 13% for Group 1, Group2, and Group 3 specimens, respectively. The theoretical values were 10% safer on average. Specimens P-NE-L and C-NE-L varied the most and the G-FRCM strengthened specimens (G-N-L, G-N-H, G-E-L, G-E-H, G-NE-L, and G-NE-H) had the closest P_u values when compared to the theoretical capacity due to the G-FRCM fabrics completely rupturing at failure.

Table 7

Calculated Load Carrying Capacity Values

No.	ID	P_u (kN)	P_{u-th} (kN)	$\frac{P_u}{P_{u-th}}$
		Reference Specimens		
1	R-L	39.9	46.3	0.86
2	R-H	99.2	100	0.99
		Group 1 Specimens		
3	P-N-L	62.7	51.6	1.21
4	C-N-L	59.2	52.8	1.12
5	G-N-L	52.4	48.7	1.08
6	P-N-H	123	104	1.18
7	C-N-H	124	106	1.17
8	G-N-H	110	106	1.04
		Group 2 Specimens		
9	P-E-L	68.9	56.9	1.21
10	C-E-L	68.7	59.0	1.16
11	G-E-L	51.9	51.8	1.00
12	P-E-H	131	119	1.11
13	C-E-H	132	120	1.10
14	G-E-H	113	114	0.99
		Group 3 Specimens		
15	P-NE-L	82.7	63.5	1.30
16	C-NE-L	83.2	66.9	1.24
17	G-NE-L	58.2	55.5	1.05
18	P-NE-H	136	128	1.06
19	C-NE-H	144	131	1.10
20	G-NE-H	124	120	1.03

CHAPTER 6: CONCLUSIONS

An experimental study was conducted to study the efficacy of the NSE-FRCM and the hybrid NSE/EB-FRCM techniques as an alternative to the traditional EB-FRCM strengthening. For this purpose, a total of 20 RC beams of dimensions 150 mm × 260 mm, 2500 mm were prepared and tested under four-point loading. The test parameters were: a) FRCM type, b) strengthening scheme, and c) reinforcement ratio. The results have been discussed in terms of load-carrying capacity, stiffness, ductility, and modes of failure. Based on the results of this investigation, the following conclusions have been made:

- The inherent surface roughening of the NSE strengthening provided a worthy alternative to sandblasting while preserving the original section shape.
- The average gain in the load carrying capacity was 62.5 % for NSE-FRCM, 72.3% for EB-FRCM, and 91.3% for NSE/EB-FRCM strengthened beams. A stiffness factor, β^f, was introduced to enable valid comparisons between the two strengthening methods. Comparing the β^f among all beams indicate an advantage for NSE strengthening considering the less amount of FRCM used in NSE than that used in the EB counterpart. It was also shown that NSE/EB strengthening provided the best FRCM utilization.
- The average initial stiffness, S_I, for the reference beams was 21 kN/mm. An increase in the initial stiffness was shown for the strengthened specimen with an average of 23.6 kN/mm ,31.6 kN/mm, and 28.1 kN/mm for specimens in Group 1 ,Group 2, and Group3, respectively. The increased height of the beam in case of EB strengthening resulted in higher initial stiffness compared to that of the NSE strengthened beams. In case of the post cracking stiffness, S_c, all beam types, NSE, EB, NSE/EB, showed comparable post-cracking stiffness.

The S_c values were 7.5 kN/mm, 6.9 kN/mm, and 7.4 kN/mm for Group 1, Group 2, and Group 3, respectively.

- All strengthened beams exhibited a reduction in ductility compared to the corresponding reference specimens. Average ΔI of 11.3, 3.9, 3.1, and 3.5 were calculated for the reference, Group 1, Group 2 and Group 3 specimens, respectively.
- All G-FRCM strengthened beams failed due to fabric rupture regardless of strengthening scheme.
- C-FRCM strengthened beams along with specimens P-N-H and P-E-H failed due to midspan FRCM delamination. Specimens P-N-H, C-E-L, and P-E-H also showed longitudinal cracks at the concrete-FRCM interface.
- The ACI 549 procedure for evaluating the ultimate load provided an average of 13%, 10%, and 13% safer prediction for NSE, EB, and NSE/EB strengthened specimens, respectively.

It is therefore recommended to perform more studies to determine the optimum width ratio that can be used in NSE strengthening and the NSE part of the hybrid strengthening to achieve maximum effectiveness. The NSE and NSE/EB strengthening are recommended over the EB strengthening technique unless it will cause the specimen to be compression controlled where other options should be investigated.

REFERENCES

[1] U. Ebead, H. El-Sherif, Near surface embedded-FRCM for flexural strengthening of reinforced concrete beams, Constr. Build. Mater. 204 (2019) 166–176. doi:10.1016/j.conbuildmat.2019.01.145.

[2] U. Ebead, Inexpensive Strengthening Technique for Partially Loaded Reinforced Concrete Beams: Experimental Study, J. Mater. Civ. Eng. (2015) 04015002. doi:10.1061/(ASCE)MT.1943-5533.0001249.

[3] M.T. El-Mihilmy, J.W. Tedesco, Analysis of Reinforced Concrete Beams Strengthened With FRP Laminates, J. Struct. Eng. 126 (2000) 684–691.

[4] R. Kotynia, H. Abdel Baky, K.W. Neale, U.A. Ebead, Flexural Strengthening of RC Beams with Externally Bonded CFRP Systems: Test Results and 3D Nonlinear FE Analysis, J. Compos. Constr. 12 (2008) 190–201. doi:10.1061/(ASCE)1090-0268(2008)12:2(190).

[5] G. Kim, J. Sim, H. Oh, Shear strength of strengthened RC beams with FRPs in shear, Constr. Build. Mater. 22 (2008) 1261–1270. doi:10.1016/j.conbuildmat.2007.01.021.

[6] A.M. Khalifa, Flexural performance of RC beams strengthened with near surface mounted CFRP strips, Alexandria Eng. J. 55 (2016) 1497–1505. doi:10.1016/j.aej.2016.01.033.

[7] C.G. Papanicolaou, T.C. Triantafillou, K. Karlos, M. Papathanasiou, Textile-reinforced mortar (TRM) versus FRP as strengthening material of URM walls: in-plane cyclic loading, Mater. Struct. 40 (2007) 1081–1097. doi:10.1617/s11527-007-9226-0.

[8] S.M. Raoof, L.N. Koutas, D.A. Bournas, Textile-reinforced mortar (TRM) versus fibre-reinforced polymers (FRP) in flexural strengthening of RC beams, Constr. Build. Mater. 151 (2017) 279–291.

doi:10.1016/j.conbuildmat.2017.05.023.

[9] Z.R. Aljazaeri, J.J. Myers, Strengthening of Reinforced-Concrete Beams in Shear with a Fabric-Reinforced Cementitious Matrix, J. Compos. Constr. 21 (2017) 1–11. doi:10.1061/(ASCE)CC.1943-5614.0000822.

[10] S. Babaeidarabad, G. Loreto, A. Nanni, Flexural Strengthening of RC Beams with an Externally Bonded Fabric-Reinforced Cementitious Matrix, J. Compos. Constr. 18 (2014) 04014009. doi:10.1061/(ASCE)CC.1943-5614.0000473.

[11] U. Ebead, H. Saeed, FRP/stirrups interaction of shear-strengthened beams, Mater. Struct. 50 (2017) 103. doi:10.1617/s11527-016-0973-7.

[12] A. Younis, U. Ebead, K.C. Shrestha, Different FRCM systems for shear-strengthening of reinforced concrete beams, Constr. Build. Mater. 153 (2017) 514–526. doi:10.1016/j.conbuildmat.2017.07.132.

[13] T.G. Wakjira, U. Ebead, Hybrid NSE/EB technique for shear strengthening of reinforced concrete beams using FRCM: Experimental study, Constr. Build. Mater. 164 (2018) 164–177. doi:10.1016/j.conbuildmat.2017.12.224.

[14] U. Ebead, K.C. Shrestha, M.S. Afzal, A. El Refai, A. Nanni, Effectiveness of Fabric-Reinforced Cementitious Matrix in Strengthening Reinforced Concrete Beams, J. Compos. Constr. 21 (2016) 04016084. doi:10.1061/(ASCE)CC.1943-5614.0000741.

[15] A. Younis, U. Ebead, Bond characteristics of different FRCM systems, Constr. Build. Mater. 175 (2018) 610–620. doi:10.1016/j.conbuildmat.2018.04.216.

[16] M. Elghazy, A. El Refai, U. Ebead, A. Nanni, Effect of corrosion damage on the flexural performance of RC beams strengthened with FRCM composites, Compos. Struct. 180 (2017) 994–1006. doi:10.1016/j.compstruct.2017.08.069.

[17] M. Elghazy, A. EL Refai, U. Ebead, A. Nanni, Corrosion-Damaged RC Beams

Repaired with Fabric-Reinforced Cementitious Matrix, J. Compos. Constr. 22 (2018). doi:10.1061/(ASCE)CC.1943-5614.0000873.

[18] M. Elghazy, A. El Refai, U. Ebead, A. Nanni, Post-repair flexural performance of corrosion-damaged beams rehabilitated with fabric-reinforced cementitious matrix (FRCM), Constr. Build. Mater. 166 (2018) 732–744. doi:10.1016/j.conbuildmat.2018.01.128.

[19] H.M. Elsanadedy, T.H. Almusallam, S.H. Alsayed, Y.A. Al-Salloum, Flexural strengthening of RC beams using textile reinforced mortar – Experimental and numerical study, Compos. Struct. 97 (2013) 40–55. doi:10.1016/j.compstruct.2012.09.053.

[20] C. Escrig, L. Gil, E. Bernat-Maso, Experimental comparison of reinforced concrete beams strengthened against bending with different types of cementitious-matrix composite materials, Constr. Build. Mater. 137 (2017) 317–329. doi:10.1016/j.conbuildmat.2017.01.106.

[21] T. El-maaddawy, A. EL Refai, Innovative Repair of Severely Corroded T-Beams Using Fabric-Reinforced Cementitious Matrix, J. Compos. Constr. 13 (2016) 04015073. doi:10.1061/(ASCE)CC.1943-5614.0000641.

[22] F. Schladitz, M. Frenzel, D. Ehlig, M. Curbach, Bending load capacity of reinforced concrete slabs strengthened with textile reinforced concrete, Eng. Struct. 40 (2012) 317–326. doi:10.1016/j.engstruct.2012.02.029.

[23] G. Loreto, L. Leardini, D. Arboleda, A. Nanni, Performance of RC Slab-Type Elements Strengthened with Fabric-Reinforced Cementitious-Matrix Composites, J. Compos. Constr. 18 (2014) A4013003. doi:10.1061/(ASCE)CC.1943-5614.0000415.

[24] ACI Committee 549, Guide to Design and Construction of Externally Bonded

Fabric-Reinforced Cementitious Matrix (FRCM) Systems for Repair and Strengthening Concrete and Masonry Structures, 2013.

[25] L. Ombres, Flexural analysis of reinforced concrete beams strengthened with a cement based high strength composite material, Compos. Struct. 94 (2011) 143–155. doi:10.1016/j.compstruct.2011.07.008.

[26] S.-P. Yin, J. Sheng, X.-X. Wang, S.-G. Li, Experimental Investigations of the Bending Fatigue Performance of TRC-Strengthened RC Beams in Conventional and Aggressive Chlorate Environments, J. Compos. Constr. 20 (2016) 04015051. doi:10.1061/(ASCE)CC.1943-5614.0000617.

[27] C. Escrig, L. Gil, E. Bernat-Maso, F. Puigvert, Experimental and analytical study of reinforced concrete beams shear strengthened with different types of textile-reinforced mortar, Constr. Build. Mater. 83 (2015) 248–260.

[28] S.M. Raoof, L.N. Koutas, D.A. Bournas, Bond between textile-reinforced mortar (TRM) and concrete substrates : Experimental investigation, Compos. Part B. 98 (2016) 350–361. doi:10.1016/j.compositesb.2016.05.041.

[29] United States Department of Labor, Protecting Workers from the Hazards of Abrasive Blasting Materials, OSHA FS 3697 - 2014, 2014.

[30] ASTM International ASTM C39/C39M-16b, Standard Test Method for Compressive Strength of Cylindrical Concrete Specimens, ASTM International, West Conshohocken, PA, 2016., 2009.

[31] ISE/104 Committee, BS 4449:2005: Steel for the reinforcement of concrete. Weldable reinforcing steel. Bar, coil and decoiled product, BSI, 2005.

[32] Ruredil, Ruredil X Mesh C10 Datasheet, 2016.

[33] Ruredil, Ruredil X Mesh Gold Datasheet, 2016.

[34] SIKA, SikaWrap -350G Grid Datasheet, 2016.

[35] ASTM C109/C109M-05, Standard Test Method for Compressive Strength of Hydraulic Cement Mortars, 2005. doi:10.1520/C0109_C0109M-05.

[36] ICC (International Code Council), Acceptance Criteria for Masonry and Concrete Strengthening Using Fabric-reinforced Cementitious Matrix (FRCM) and Steel Reinforced Grout (SRG) Composite Systems - AC434, ICC Evaluation Service, 2016.

[37] T.G. Wakjira, U. Ebead, FRCM/internal transverse shear reinforcement interaction in shear strengthened RC beams, Compos. Struct. 201 (2018) 326–339. doi:10.1016/j.compstruct.2018.06.034.

[38] ACI Committee 318, Building code requirements for structural plain concrete (ACI 318.1-83) and commentary, 2014.

APPENDIXES

Appendix A: Theoretical load carrying capacity example calculation

Specimen G-E-H has the following properties:

- $h = 260\ mm,\ b = 150\ mm,\ d_s = 210\ mm,\ d'_s = 30\ mm,\ A_s = 402\ mm^2$
- $F_{y\,10} = 594.5\ MPa,\ E_{s\,10} = 205,\ A'_s = 100\ mm^2$
- $A_f = 0.047\frac{mm^2}{mm},\ E_f = 60\ GPa,\ b_f = 150\ mm,\ d_f = 267.5\ mm, n = 2$

$$\varepsilon_{fe} = 0.0093\ < 0.012$$

Let $c_u = 50\ mm$

$$\varepsilon_c = \varepsilon_{fe}\left(\frac{c_u}{d_f - c_u}\right) = 0.0093\left(\frac{50}{267.5 - 50}\right) = 0.00214$$

$$\varepsilon_t = \varepsilon_{fe}\left(\frac{d - c_u}{d_f - c_u}\right) = 0.0093\left(\frac{210 - 50}{267.5 - 50}\right) = 0.00684$$

$$\varepsilon'_s = \varepsilon_c\left(\frac{c_u - d'}{c_u}\right) = 0.00214\left(\frac{50 - 30}{50}\right) = 0.000856$$

$$T_s = A_s f_y - A'_s E_s \varepsilon'_s = 405 \times 594.5 - 100 \times 205000 \times 0.000856 = 223.2\ kN$$

$$T_f = nA_f b_f E_f \varepsilon_{fe} = 2 \times 0.047 \times 150 \times 60000 \times 0.0093 = 7.9\ kN$$

$$\varepsilon'_c = 1.7\frac{f'_c}{E_c} = 1.7 \times \frac{39.5}{29539} = 0.00227$$

$$\beta_1 = \frac{4\varepsilon'_c - \varepsilon_c}{6\varepsilon'_c - 2\varepsilon_c} = \frac{4 \times 0.00227 - 0.00214}{6 \times 0.00227 - 2 \times 0.00214} = 0.74$$

$$\alpha_1 = \frac{3\varepsilon'_c\varepsilon_c - \varepsilon_c^2}{3\beta_1{\varepsilon'_c}^2} = \frac{3 \times 0.00227 \times 0.00214 - 0.00214^2}{3 \times 0.74 \times 0.00227^2} = 0.87$$

The new estimated value of c_u is calculated as follows:

$$c_{u-new} = \frac{T_s + T_f}{\alpha_1 f'_c \beta_1 b} = \frac{(223.2 + 7.9) \times 1000}{0.87 \times 0.74 \times 39.5 \times 150} = 60.6\ mm$$

$$Error = \frac{60.6 - 50}{50} = 21.2\%$$

Instead of using the newly estimated value, we will assume $c_u = 55\ mm$

$$\varepsilon_c = \varepsilon_{fe}\left(\frac{c_u}{d_f - c_u}\right) = 0.0093\left(\frac{55}{267.5 - 55}\right) = 0.00241$$

$$\varepsilon_t = \varepsilon_{fe}\left(\frac{d - c_u}{d_f - c_u}\right) = 0.0093\left(\frac{210 - 55}{267.5 - 55}\right) = 0.00678$$

$$\varepsilon_s' = \varepsilon_c\left(\frac{c_u - d'}{c_u}\right) = 0.00241\left(\frac{55 - 30}{55}\right) = 0.00109$$

$$T_s = A_s f_y - A_s' E_s \varepsilon_s' = 405 \times 594.5 - 100 \times 205000 \times 0.00109 = 218.4\ kN$$

$$T_f = nA_f b_f E_f \varepsilon_{fe} = 2 \times 0.047 \times 150 \times 60000 \times 0.0093 = 7.9\ kN$$

$$\beta_1 = \frac{4\varepsilon_c' - \varepsilon_c}{6\varepsilon_c' - 2\varepsilon_c} = \frac{4 \times 0.00227 - 0.00241}{6 \times 0.00227 - 2 \times 0.00241} = 0.76$$

$$\alpha_1 = \frac{3\varepsilon_c'\varepsilon_c - \varepsilon_c^2}{3\beta_1 {\varepsilon_c'}^2} = \frac{3 \times 0.00227 \times 0.00241 - 0.00241^2}{3 \times 0.76 \times 0.00227^2} = 0.9$$

$$c_{u-new} = \frac{T_s + T_f}{\alpha_1 f_c' \beta_1 b} = \frac{(218.4 + 7.9) \times 1000}{0.9 \times 0.76 \times 39.5 \times 150} = 55.83\ mm$$

$$Error = \frac{55.82 - 55}{55} = 1.5\%$$

Which shows that 55 mm is very close to the true value. We will $c_u = 55.2\ mm$ so that the error becomes closer to 1%.

$$\varepsilon_c = \varepsilon_{fe}\left(\frac{c_u}{d_f - c_u}\right) = 0.0093\left(\frac{55.2}{267.5 - 55.2}\right) = 0.00242$$

$$\varepsilon_t = \varepsilon_{fe}\left(\frac{d - c_u}{d_f - c_u}\right) = 0.0093\left(\frac{210 - 55.2}{267.5 - 55.2}\right) = 0.00678$$

$$\varepsilon_s' = \varepsilon_c\left(\frac{c_u - d'}{c_u}\right) = 0.00242\left(\frac{55.2 - 30}{55.2}\right) = 0.00110$$

$$T_s = A_s f_y - A_s' E_s \varepsilon_s' = 405 \times 594.5 - 100 \times 205000 \times 0.00110 = 218.2\ kN$$

$$T_f = nA_f b_f E_f \varepsilon_{fe} = 2 \times 0.047 \times 150 \times 60000 \times 0.0093 = 7.9\ kN$$

$$\beta_1 = \frac{4\varepsilon_c' - \varepsilon_c}{6\varepsilon_c' - 2\varepsilon_c} = \frac{4 \times 0.00227 - 0.00242}{6 \times 0.00227 - 2 \times 0.00242} = 0.759$$

$$\alpha_1 = \frac{3\varepsilon_c'\varepsilon_c - \varepsilon_c^2}{3\beta_1 {\varepsilon_c'}^2} = \frac{3 \times 0.00227 \times 0.00242 - 0.00242^2}{3 \times 0.76 \times 0.00227^2} = 0.904$$

$$c_{u-new} = \frac{T_s + T_f}{\alpha_1 f_c' \beta_1 b} = \frac{(218.2 + 7.9) \times 1000}{0.904 \times 0.759 \times 39.5 \times 150} = 55.61\ mm$$

$$Error = \frac{55.61 - 55}{55} = 1.1\%$$

This c_u value will therefore be used for the calculation.

$$M_s = A_s f_y \left(d - \frac{\beta_1 c_u}{2}\right) + A_s' E_s \varepsilon_s' (d - d')$$

$$= 402 \times 594.5 \times \left(210 - \frac{0.759 \times 55.2}{2}\right)$$

$$+ 100 \times 205 \times 0.0011 \times (210 - 30) = 49240252\ N.mm$$

$$= 45.2\ kN.m$$

$$M_f = T_f \left(d_f - \frac{\beta_1 c_u}{2}\right) = 7.9 \times \left(267.5 - \frac{0.759 \times 55.2}{2}\right) = 2047\ kN.mm$$

$$= 2.05\ kN.m$$

$$P_{u-th} = \frac{2M_u}{l} = \frac{2(45.2 + 2.05)}{0.825} = 114\ kN$$